



1 **An investigation on the origin of regional spring time ozone**
2 **episodes in the Western Mediterranean and Central Europe**

3 Pavlos Kalabokas^{1,2}, Jens Hjorth², Gilles Foret³, Gaëlle Dufour³, Maxim Eremenko³,
4 Guillaume Siour³, Juan Cuesta³, Matthias Beekmann³

5 ¹Academy of Athens, Research Center for Atmospheric Physics and Climatology, Athens, Greece

6 ²European Commission, Joint Research Centre (JRC), Institute for Environment and Sustainability (IES), Air
7 and Climate Unit, I - 21027 Ispra (VA), Italy

8 ³Laboratoire Inter-universitaire des Systèmes Atmosphériques (LISA), Universités Paris-Est Créteil et Paris
9 Diderot, CNRS, Créteil, France

10 *Correspondence to:* Pavlos Kalabokas (pkalabokas@academyofathens.gr)

11

12 **Abstract.** For the identification of regional spring time ozone episodes, rural EMEP ozone measurements from
13 countries surrounding the Western Mediterranean (Spain, France, Switzerland, Italy, Malta) have been examined
14 with emphasis on periods of high ozone concentrations, according to the daily variation of the afternoon (12:00 –
15 18:00) ozone values. For two selected high ozone episodes in April and May 2008, composite NCEP/NCAR
16 reanalysis maps of various meteorological parameters and/or their anomalies (geopotential height, specific
17 humidity, vertical wind velocity omega, vector wind speed and temperature) at various tropospheric pressure
18 levels have been examined together with the corresponding satellite IASI ozone measurements (at 3 and 10 km),
19 CHIMERE simulations, vertical ozone soundings and HYSPLIT back trajectories. The results show that high
20 ozone values are detected in several countries simultaneously over several days. Also, the examined spring
21 ozone episodes over the Western Mediterranean and in Central Europe are linked to synoptic meteorological
22 conditions very similar to those recently observed in summertime ozone episodes over the Eastern
23 Mediterranean (Kalabokas et al., ACP, 2013; Doche et al., ACP, 2014; Kalabokas et al., TellusB, 2015), where
24 the transport of tropospheric ozone-rich air masses through atmospheric subsidence influences significantly the
25 boundary layer and surface ozone concentrations. In particular, the geographic areas with observed tropospheric
26 subsidence seem to be the transition regions between high pressure and low pressure systems. Over these areas,
27 strong gradients of geopotential height and temperature are observed, together with high positive omega vertical
28 wind velocity (downward transport) and low specific humidity (dry conditions), at all examined pressure levels
29 below the altitude of 500 hPa pressure level. During the surface ozone episodes IASI satellite measurements
30 show extended areas of high ozone in the lower and upper troposphere over the low pressure system areas,
31 adjacent to the anticyclones, which influence significantly the boundary layer and surface ozone concentrations
32 within the anticyclones by subsidence and advection in addition to the photochemically produced ozone there,
33 resulting in exceedances of the 60 ppb standard.

34



1 **1 Introduction**

2 Surface ozone is a pollutant harmful to both human health and vegetation (Levy et al., 2001; Fuhrer, 2009).
3 Further, in the upper troposphere ozone acts as a powerful greenhouse gas (IPCC, 2007). The concentrations of
4 ozone throughout the troposphere depend on the meteorological conditions driving vertical and horizontal
5 transport and on photochemical ozone production from its precursors, nitrogen oxides (NO_x) volatile organic
6 compounds (VOCs) and carbon monoxide (Delmas et al., 2005; Seinfeld and Pandis, 2006; Monks et al., 2015).

7 The European network of surface ozone monitoring stations shows persistently exceedances of the European
8 long-term target value for protection of human health, under anticyclonic synoptic meteorological conditions
9 during the warm season in southern and central Europe (EEA, 2015). The Mediterranean area is particularly
10 exposed to ozone pollution because of the combination of the specific meteorological conditions prevailing
11 during spring and summer and the regional air pollutant emissions. Data collected from air pollution monitoring
12 stations in combination with results of measurement campaigns show that ozone concentrations in the
13 Mediterranean Basin are relatively high: Lelieveld et al. (2002) found that summer ozone concentrations over the
14 Mediterranean are a factor of 2.5–3 higher than in the hemispheric background troposphere, in the boundary
15 layer and up to 4 km altitude. Rural stations in continental Greece, Italy, Malta and eastern Spain report summer
16 average ozone values of about 60–70 ppbv, significantly higher than values in Northern and Western Europe
17 (Bonasoni et al., 2000; Kalabokas et al., 2000; Millan et al., 2000; Kourtidis et al., 2002; Kouvarakis et al., 2002;
18 Nolle et al., 2002; Kalabokas and Repapis, 2004; Paoletti, 2006; Sánchez et al., 2008; Schürmann et al., 2009;
19 Velchev et al., 2011; Kalabokas et al., 2008; Kleanthous et al., 2014; Cristofanelli et al., 2015). Results from 3-
20 D chemistry transport models also suggest that ozone concentrations are higher than for the rest of Europe (e.g.
21 Johnson et al., 2001). High ozone values in the Mediterranean are typical not only for ground level
22 measurements, but for the entire boundary layer as well as the entire lower troposphere (Millan et al., 1997,
23 2000; Kalabokas et al., 2007).

24 The Mediterranean climate with frequent anticyclonic, clear sky conditions in spring and summer favours
25 photochemical ozone formation in the troposphere. Furthermore, Mediterranean tropospheric ozone levels are
26 influenced by long-range transport of ozone and its precursors from Europe, Asia and even North America as
27 well as emissions of precursors from sources around the Basin, particularly the large cities (Lelieveld et al.,
28 2002; Gerasopoulos, 2005; Safieddine et al., 2014). Also natural VOC emissions in the area have been found to
29 be important ozone precursors (Richards et al., 2013). Studies in the Western part of the Mediterranean highlight
30 the role of the breeze circulation in accumulation of high ozone levels (Millan et al., 1997, 2000).

31 Anticyclones are generally linked to atmospheric subsidence, which seems to be particularly important over the
32 Eastern Mediterranean as a cause of elevated ozone concentrations. During the summer period, the
33 Mediterranean area is directly under the descending branch of the Hadley circulation, caused by deep convection
34 in the tropics (Lelieveld, 2009). However a main reason for the strong subsidence observed in the Mediterranean
35 Basin appears to be an impact of the Indian monsoon, inducing a Rossby wave that by the interaction with the
36 midlatitude westerlies produces adiabatic descent in the area (Rodwell and Hoskins, 1996, 2001; Tyrlis et al.,
37 2013). In general, in the Eastern Mediterranean strong deep subsidence in the lower troposphere influencing the
38 boundary layer has been documented, based essentially on the analysis of MOZAIC vertical ozone profiles as



1 well as surface ozone and satellite measurements (Kalabokas et al., 2007; Kalabokas et al., 2008; Eremenko et
2 al., 2008; Foret et al., 2009; Liu et al., 2009; Kalabokas et al., 2013; Doche et al., 2014; Kalabokas et al., 2015).
3 Also data analysis based on large-scale atmospheric modeling studies (Li et al., 2001; Richards et al., 2013; Zanis
4 et al., 2014; Safieddine et al., 2014; Tyrlis et al., 2014) shows the importance of vertical transport of ozone in the
5 Mediterranean area, particularly in its eastern part.

6 Recent research based on vertical MOZAIC ozone profiles (Kalabokas et al., 2015) suggests that during days
7 with the highest ozone levels for both the free lower troposphere (1.5-5 km) and the boundary layer (0-1.5 km)
8 over the middle-eastern airports of Cairo and Tel-Aviv there are extended regions of strong subsidence in the
9 Eastern Mediterranean but also in Eastern and Northern Europe and over these regions the atmosphere is dryer
10 than average.

11 The influence of tropospheric transport of ozone at hemispheric scale, on surface ozone concentrations, is an
12 issue of potential importance to ozone abatement policies. Vertical transport of ozone is of particular relevance
13 to the ozone transport over long distances in the troposphere because the lifetime of ozone in the free
14 troposphere is longer and the transport times are typically shorter than in the boundary layer (HTAP, 2010). The
15 impact on surface ozone of the long range transport of ozone has been extensively investigated in the US, where
16 a clear difference has been observed between the eastern part, where surface ozone concentrations have
17 decreased very significantly, and the western part, where most sites do not show such a trend, apparently due to
18 the effects of transport (Cooper et al., 2012). Studies based on observations and trajectory modelling indicate
19 that transport above the boundary layer and entrainment of ozone from the free troposphere has an important
20 impact on surface ozone concentrations at several sites in the western US (Cooper et al., 2011; Langford et al.,
21 2015). Also a changing seasonal cycle of ozone, with a tendency towards a maximum earlier in the year, has
22 been tentatively explained by the influence of atmospheric transport patterns combined with a change in the
23 temporal and spatial emissions of ozone precursors (Parrish et al., 2013).

24 The importance of hemispheric transport for Mediterranean air pollution in particular has previously been
25 highlighted in the modelling study by Stohl et al. (2002) of intercontinental transport of air pollutants, who found
26 the highest concentrations of a passive tracer for North American emissions in the Mediterranean Basin. The
27 modelling studies of Richard et al. (2013) and Safieddine et al. (2014) both come to the conclusion that the
28 emission sources within the Mediterranean area have a dominating influence on surface ozone while remote
29 sources, e.g. in Asia and North America, are more important than local sources for ozone concentrations at
30 higher altitudes (above 700 hPa according to Richards et al. 2013). The radiative (climate) impact of ozone
31 depends mainly on the concentrations above the boundary layer. Relatively high ozone concentrations are
32 reported in the Central Mediterranean also during the winter-early spring period (Nolle et al., 2002) while, in an
33 extended observational study in the Western Mediterranean basin a converging trend between the background
34 rural ozone values and the urban ozone values was reported (Sicard et al., 2013).

35 Most studies of Mediterranean ozone have been focused on the Eastern part of the Mediterranean basin where
36 the influence of downwards transport appears to be more important than it is in the Central and Western part,
37 although also at this part of the Mediterranean very frequently anticyclonic conditions dominate in spring and
38 summer months. The mechanisms governing ozone levels in the Western and Central Mediterranean appear to



1 need further clarification. For example, in Kalabokas et al. (2008) as well as in the more recent study by Zanis et
2 al. (2014) it was found that rural background ozone monitoring stations in the Western and Central
3 Mediterranean show climatological spring time ozone maximum in April-May while the corresponding rural
4 background ozone Eastern Mediterranean stations, have their climatological maxima in July-August. Also, in
5 Eastern Greece and the Aegean Sea the summer rural background ozone levels are systematically higher than the
6 corresponding ones observed in the Central Mediterranean (Malta) and the Eastern Mediterranean (Cyprus). The
7 above is contrary to the predictions of a model simulation that suggested a rather uniform ozone distribution
8 across the basin (Zanis et al., 2014). Understanding the origin of high ozone levels during spring time is
9 particularly challenging because this is a period where photochemical formation in the troposphere is increasing
10 due to rising sun intensity, but also stratospheric intrusions may be of relevance as these have been found to have
11 a maximum in Southern Europe in spring/early summer (Beekmann et al., 1994; Monks, 2000).

12 The focus of the present study thus is to improve the understanding of ozone behaviour over the Western
13 Mediterranean and the surrounding area to the north part of the basin, towards central Europe in the springtime.
14 In particular, it aims at investigating to which extend surface ozone concentrations during the high ozone
15 episodes are influenced by entrainment of ozone rich air and how much the episodes depend on ozone formation
16 in the boundary layer. Further, this study investigates the factors controlling ozone distribution in the free
17 troposphere, particularly transport within the troposphere, stratosphere-troposphere exchange and photochemical
18 formation in the free troposphere. Two episodes in late April and early May have been selected for a detailed
19 analysis. We analyze the two spring time episodes of high surface ozone concentrations over the Western
20 Mediterranean and the surrounding area using a comprehensive combination of surface observations, Infrared
21 Atmospheric Sounding Interferometer (IASI) satellite observations, meteorological maps, back trajectories and
22 regional air quality modelling to understand the principal mechanisms contributing to these events.

23

24 **2 Data and methodology**

25 The following data will be used in the analysis:

26 1) Ozone measurements from the European Monitoring and Evaluation Programme (EMEP) and European
27 Environment Agency (EEA) air pollution network

28 The surface ozone measurements during spring 2008 (March-May) of some EMEP rural ozone stations
29 surrounding the western Mediterranean basin [Spain (ES10), France (FR10, FR14), Switzerland (CH02, CH04),
30 Italy (IT01, IT04), Malta (MT01)] have been analyzed with emphasis on periods of high ozone, focused mostly
31 on the daily variation of the daily mean afternoon (12:00 – 18:00) ozone values. In addition, during the selected
32 spring ozone episodes the measurements of the EEA air pollution network are also taken into account for the
33 analysis.

34 2) Composite NCEP/NCAR Reanalysis maps

35 Composite or daily NCEP/NCAR reanalysis meteorological maps covering Europe and N. Africa and
36 corresponding to periods of high ozone have been plotted for the following meteorological parameters:
37 Geopotential height, specific humidity anomaly, vertical wind velocity Omega (and anomaly), vector wind speed



1 and temperature anomaly. The examination was focused on the tropospheric pressure levels at 850, 700 and
2 500hPa levels (for space limitations mainly the 850hPa charts are presented). The charts are based on grids of
3 2.5×2.5 degrees, following the procedure of Kalnay et al. (1996).

4 3). HYSPLIT back trajectories

5 Six-day back trajectories were calculated with end points at 50, 500 and 1500 meter altitude, using the NOAA
6 HYSPLIT model with GDAS meteorological data (Draxler and Rolph, 2015) for the EMEP stations and the days
7 of the selected ozone episodes. The GDAS data have a horizontal resolution of 1 degree and 23 vertical levels
8 between 1000 and 20 hPa.

9 4). Satellite IASI ozone measurements

10 Satellite observations provide interesting possibilities to support the analysis of ground measurements as well as
11 modeling simulations. Indeed, during the last decade, satellite observations of tropospheric ozone have been
12 developed and have become more and more precise (e.g. Fishman et al., 2003; Liu et al., 2005; Coheur et al.,
13 2005; Worden et al., 2007; Eremenko et al., 2008). These observations are now able to complement in situ
14 observations, offering wide spatial coverage and good horizontal resolution.

15 The IASI instrument (Clerbaux et al., 2009), on board the MetOp-A platform since 19 October 2006, is a nadir-
16 viewing Fourier transform spectrometer operating in the thermal infrared between 645 and 2760 cm^{-1} with an
17 apodized spectral resolution of 0.5 cm^{-1} . The IASI field of view is composed of a 2×2 matrix of pixels with a
18 diameter at nadir of 12 km each. IASI scans the atmosphere with a swath width of 2200 km, allowing the
19 monitoring of atmospheric composition twice a day at any (cloud-free) location. The spectral coverage and the
20 radiometric and spectral performances of IASI allow this instrument to measure the global distribution of several
21 important atmospheric trace gases (e.g. Boynard et al., 2009; George et al., 2009; Clarisse et al., 2011). As in
22 Doche et al. (2014), IASI data at 3 and 10 km height are used here for analysis. These levels are representative
23 for the lower and upper troposphere respectively. However, due to the limited vertical sensitivity and resolution
24 of IASI, ozone concentrations retrieved at 3 km describe the ozone variability from roughly 2 to 8 km, and ozone
25 concentrations retrieved at 10 km describe the ozone variability from 5 to 14 km (Dufour et al., 2010). Despite
26 this overlapping, recent studies show that uncorrelated information from the lower and the upper troposphere can
27 be derived from IASI (Dufour et al., 2010, 2012, 2015).

28 5) Vertical ozone soundings

29 Further information about the vertical ozone distribution is obtained from the ozone soundings made from the
30 site of Payerne, Switzerland, Uccle, Belgium and Hohenpeissenberg, Germany. These are regularly carried out
31 with balloon launches starting at 11 AM UTC using ECC (Electrochemical Concentration Cell) ozonesondes in
32 Payerne and Uccle and Brewer-Mast ozonesondes in Hohenpeissenberg. The data were downloaded from the
33 website of the World Ozone and Ultraviolet Data Centre (WOUDC, 2015), uncertainties on the measured ozone
34 concentrations for ECC ozonesondes are between 5 and 10% (Rene Stübi, personal communication).

35 6). Regional air quality simulations



1 The CHIMERE model (Menut et al, 2013) is a state-of-the-art model widely used for pollution and air quality
2 studies (Rouil et al., 2009; Beekmann and Vautard, 2010). For the purpose of this study, we have used a version
3 of the model covering a western European domain (35° N – 70° N latitude, 15° W - 35° E longitude). The whole
4 troposphere is described from ground to about 200 hPa using 30 hybrid (sigma, P) levels. The meteorological
5 forcing is given by the IFS forecast of the ECMWF based each day on the 0 and 12 am analysis. The
6 anthropogenic emissions are prescribed by using the TNO inventory (Kuenen et al, 2014) while natural
7 emissions are calculated by the MEGAN module (Guenther et al, 2006). A passive tracer has been used to
8 analyse the dynamics patterns responsible for ozone transport, which is initialized and emitted in the top model
9 layer (11-12 km) i.e within the upper troposphere every hour. A 10- day period (spin-up period) is simulated
10 before each targeted period to establish a kind of equilibrium state of the tracer. Moreover, simulations have also
11 been made by switching off emissions for both periods under study. Differences between simulations with and
12 without emissions is a proxy of the photochemical production of ozone within the boundary layer.

13 The methodology used in this paper is the following:

14 At first, in order to minimize local pollution effects and focus on boundary layer ozone measurements
15 representative of a wider geographical area than the station location, only the afternoon (12:00 – 18:00) ozone
16 concentrations, typically representing a well-mixed boundary layer, have been analyzed.

17 Also, recent observations over the Mediterranean both from MOZAIC tropospheric ozone profiles (Kalabokas et
18 al., 2013) as well as satellite data (Zanis et al., 2014) show a strong anticorrelation between ozone and
19 atmospheric humidity. Therefore, in dry and descending air masses originating from the upper tropospheric
20 layers, higher tropospheric ozone levels would be expected. It is well known that the concentration of water
21 vapour in the troposphere (specific humidity) tends to decrease with increasing altitude because the lower air
22 temperatures at higher altitudes cause elimination of water vapour by condensation followed by precipitation.
23 This makes specific humidity an indicator of subsiding air masses, which will be used in the analysis.

24 In addition, previous research carried out in the Mediterranean (Kalabokas et al., 2007; Kalabokas et al., 2008;
25 Velchev et al., 2011; Kalabokas et al., 2013; Kalabokas et al., 2015) suggested that there is a strong link between
26 synoptic meteorology conditions and ozone concentration variability.

27 Based on the above, a systematic investigation of the composite meteorological maps (NCEP/NCAR Reanalysis)
28 during two spring high ozone episodes at the 850 hPa pressure level was carried out, until 5 days before the
29 event for the meteorological parameters mentioned previously. The purpose of the analysis is to identify areas of
30 high subsidence in the free troposphere, which could potentially influence the examined surface ozone
31 measurements, considering also that the afternoon (12:00 – 18:00) ozone concentrations are quite representative
32 of the boundary layer values. The high subsidence areas were detected in the first place by the positive vertical
33 velocity omega (and anomalies) as well as the negative specific humidity anomalies. Also, the geographical
34 distributions of geopotential heights, temperature anomalies and vector wind speed were very useful in the
35 examination of the influence of synoptic meteorological conditions on ozone concentrations. In addition, air
36 mass back trajectories (NOAA HYSPLIT), satellite IASI ozone measurements at the 3km and 10km levels,
37 afternoon surface ozone measurements from the EEA European network and vertical ozone profile
38 measurements in Central Europe during a selected ozone episode, were used for the analysis. Finally, CHIMERE



1 tracer simulations and modelling of ozone field for the April and May 2008 ozone episodes have been performed
2 for the validation of the analysis of measurement data.

3

4 **3 Results and discussion**

5 **3.1 Surface Ozone measurements in the Western Mediterranean basin in spring 2008**

6 In Fig. 1 (upper panel) the afternoon (12:00 – 18:00) rural ozone concentrations of selected EMEP stations from
7 countries surrounding the Western Mediterranean basin (Spain, France, Switzerland, Italy, Malta) during spring
8 (March – May) 2008 have been plotted. A first investigation of the plots leads to the following remarks:

9 a). Episodic periods of high ozone (and also for low ozone) may last for several days and they can be detected
10 simultaneously in many countries surrounding the western Mediterranean basin.

11 b). The 60 ppb ($120 \mu\text{g}/\text{m}^3$) EU standard for human health protection can be exceeded over many days and in
12 many countries.

13 From the above stations, the ozone concentrations measured at the EMEP stations in France and Switzerland as
14 well as the EMEP station in Northern Italy (IT04, JRC-Ispra), presented in Fig. 1 (lower panel), show generally a
15 very good agreement between each other. This feature is remarkable given their different site characteristics, the
16 large distance between them as well as their location relative to the huge natural barrier of the Alpine
17 mountainous area. So, the high mid-day ozone concentrations observed simultaneously over many countries
18 could be considered as regional ozone episodes. The two regional spring 2008 ozone episodes with the highest
19 ozone concentrations in the examined area were on 26-27 April, 2008 and 7-9 May, 2008; they have been
20 selected for further analysis.

21

22 **3.2 Geographical distribution of meteorological parameters, IASI tropospheric ozone measurements and 23 CHIMERE modelling tracer simulations during the April 26-27, 2008 ozone episode**

24 The composite NCEP/NCAR Reanalysis maps at 850 hPa for the high ozone episode of April 26-27, 2008 (and
25 also 2, 3 and 5 days before) are presented in Fig. 2 (geopotential height/specific humidity anomaly), Fig. 3
26 (vertical velocity omega/vertical velocity omega anomaly) and Fig. 4 (temperature anomaly/vector wind speed).
27 The corresponding composite maps at the 700hPa and 500 hPa pressure levels have also been plotted and
28 analyzed (not shown). The examination of these meteorological charts leads to the following remarks:

29 a). The anticyclone located to the west of the N. African coast is progressively strengthening and expanding after
30 April 23-24, 2008 while moving rapidly towards the European continent. At the same time the low pressure
31 system installed over E. Europe on April 21-24 is progressively reduced to a cut-off low on April 26-27 while
32 moving towards Greece and Turkey (Fig. 2).



1 b). Negative specific humidity anomalies are observed all over N. and E. Europe as well as over the Atlantic
2 Ocean while at the peak of the episode (April 26-27) the dry air masses prevail over a vast and extended area
3 from Russia to NW Africa and the Atlantic (Fig. 2).

4 c). An extended area of positive vertical velocity omega (and anomalies), which is a direct sign of subsiding air
5 masses, is observed over the W. Mediterranean and the Atlantic and is moving rapidly towards the Central
6 Mediterranean. Five days before the episode (April 21-22) the maximum of subsidence area was observed over
7 the Iberian Peninsula and the adjacent ocean up to the Canary islands. Then it is moving rapidly eastwards,
8 showing a maximum over Italy at the peak of the episode (April 26-27) as well as a secondary maximum over
9 Germany (Fig. 3). The positive omega anomalies indicate that the observed subsidence during the episode days
10 is higher than usual for this period of the year and the examined geographical regions.

11 d). A strong westerly flow is observed over the Western Mediterranean region of subsidence with the air masses
12 originating from the region of N. Atlantic where a deep and extended low pressure system is observed (Fig. 4).
13 As seen, the extension of the N. African anticyclone towards the Western Mediterranean changes progressively
14 the very strong westerly flow (observed 5 days before the episode, April 21-22) to a strong north-westerly. Also,
15 strong N-NW winds over the Central Mediterranean prevail at the interface area between the cut-off low and the
16 anticyclone.

17 e). Strong and extended negative temperature anomalies are observed 5 days before the episode over the Iberian
18 peninsula and the adjacent N. African coast, moving towards the Central Mediterranean and the Libyan coast.
19 The negative temperature anomaly area becomes more extended during the episode days, indicating that colder
20 atmospheric conditions than the normal prevail during the ozone episode over the corresponding areas, while
21 during photochemical ozone episodes higher than normal air temperatures would be expected. This can be
22 explained as an impact of transport of cold air masses to these areas.

23 Overall, over the same area of subsidence, strong winds together with positive omega vertical velocity (and
24 anomalies) are observed as well as negative humidity anomalies, thus indicating a strong descending air current,
25 which transports rapidly tropospheric air towards the boundary layer.

26 In Figure 5, the composite ozone IASI measurements from April 21, 2008 to April 27, 2008 are presented at two
27 altitude levels (3 km and 10 km), which are considered representative for the lower and the upper troposphere
28 (Doche et al., 2014), even if a partial overlap occurs due to reduced resolution (see section 2). An extended area
29 of very high ozone in the upper and lower troposphere is observed over the N. Atlantic over the area covered by
30 the low pressure system. At the same time, in the Central Mediterranean a high tropospheric ozone area is
31 progressively formed at both examined tropospheric layers (3 and 10 km) and having its maximum on April 26-
32 27. This observation could be associated with the information extracted from the analysis of the composite
33 meteorological charts over this Central Mediterranean area where clear indications of very strong subsidence of
34 dry air masses is observed together with very strong north-westerly winds recorded over the Mediterranean at
35 850hPa (Figs 2-4), especially for April 26-27. The same features are also observed at the pressure levels of
36 700hPa and 500 hPa (not shown).

37 For a more detailed analysis during the maximum of the episode (April 26-27), in Fig. 6 the daily IASI satellite
38 ozone measurements at 3 and 10 km altitude are presented in a higher concentration resolution as well as in a



1 more restricted geographical domain (same as the CHIMERE simulation outputs), where the above described
2 characteristics of the geographical distribution of tropospheric ozone appear more clear. Also, for a more
3 detailed investigation of the corresponding meteorological characteristics at higher tropospheric levels, in Fig. 7
4 the daily meteorological charts of columnar precipitable water anomaly and geopotential heights at 500hPa and
5 700hPa for April 26 and 27, 2008 are presented. The very extended areas with negative columnar precipitable
6 water anomalies show that the dry conditions, indicating subsidence, prevail over the whole troposphere, mostly
7 over its lower part, over a vast area and especially at the interface areas of the high and low pressure systems at
8 500 hPa, very similar to what was already observed at 850 hPa (Fig. 2). So, it comes out that during the ozone
9 episode the same synoptic pattern is observed in the troposphere up to 500 hPa (Fig. 7) but even at higher levels
10 (not shown).

11 In order to study in more detail the atmospheric processes prevailing during the examined April ozone episode
12 and complete the analysis of the dynamic atmospheric conditions during the examined events, regarding more
13 specifically the origin of ozone measured in the boundary layer, we have performed simulations with the
14 CHIMERE model using tracers to analyze transport patterns. The results of the CHIMERE simulations for the
15 April episode are shown in Figs 8-9, where simulations of upper tropospheric tracer concentrations, simulations
16 of photochemical production and simulations of the ozone field (together with the iso-contours of the high
17 tropospheric tracer) are presented. As described earlier (cf Chapter 2), we use a tracer initialized within the
18 model top layer in the upper troposphere at about 11 km height. Inspecting qualitatively simulated
19 concentrations at 3 km and 1.5 km altitude (Fig. 8, 9), it is shown that the upper tropospheric tracer is present at
20 these levels, indicating significant downward transport or upper troposphere air masses to the boundary layer,
21 which coincides with the maximum concentrations of the CHIMERE simulated ozone field at 3 and 1.5 km
22 covering a large area from Switzerland to Malta (Fig. 9). Combining that with the meteorological charts (Figs 2,
23 7), on the outer side of the low-pressure area and at the interface with the N. African anticyclone high values of
24 the upper tropospheric tracer indicating considerable subsidence are observed at 5 km altitude (not shown),
25 which becomes even stronger and more extended at the 3 km and 1.5 km altitudes (Fig.9). So, following the
26 geographical distribution of the upper tropospheric tracer at 3 km and 1.5 km (Fig.9), tropospheric subsidence is
27 observed at the periphery of the anticyclonic area and at the interface with the low-pressure area. Therefore, the
28 downward transport of upper tropospheric ozone is influencing the boundary layer over the examined location.
29 The observed patterns, based on CHIMERE tracer simulations and on ozone concentrations are quite consistent
30 with the observed values of the IASI instrument that show the same structures, in particular enhanced
31 concentrations at 3km over Italy (Figs 5,6), as well as with the analysis of meteorological parameters based on
32 composite charts (Figs 2-4) and described above. Regarding the comparison of the geographical distribution of
33 the CHIMERE ozone field (Fig.9) with the IASI measurements at 3 km or 700hPa (Figs 5-6), a clear difference
34 over the N. Atlantic and over the Central Mediterranean is observed. As discussed above, in both regions the
35 prevailing meteorological conditions (low pressure systems) are associated with high tropospheric ozone levels.
36 It has to be mentioned that direct comparison of CHIMERE simulations at 3 km with the corresponding IASI
37 measurements presents some weaknesses, especially due to the fact that IASI is sensitive to a height range
38 between 2 and 8 km and the IASI averaging kernels need to be applied to CHIMERE to make it comparable with
39 IASI (Eremenko et al., 2008).



1 The graphical representation on the map of the daily evolution of the hourly surface ozone concentrations at
2 15:00 h as recorded in the air pollution stations of the EEA-AirBase network (EEA, 2015) during the 26-27
3 April period (Fig. 9) shows very high concentrations, exceeding 70 ppb, appearing at many locations in Spain as
4 well as in S. France and NW Italy. As mentioned previously, during the afternoon hours the influence of the free
5 troposphere on the boundary layer is maximized through vertical mixing, and the composite meteorological
6 maps show a large corridor of subsiding dry air masses over the same area (Figs 2-4), which is a very strong
7 indication that the surface ozone concentrations could be influenced by entrainment of subsiding ozone-rich air.
8 The CHIMERE tracer simulations suggest that in this case the subsiding air masses are not coming directly from
9 the upper troposphere.

10 The HYSPLIT back-trajectories during the April episode arriving at the EMEP stations in Italy (JRC-Ispra) and
11 on Malta (Fig. 10) show in fact subsiding air masses arriving from northern directions, on April 25 and 26 for
12 Ispra and on April 27 for Malta and give more or less the same picture as the Swiss stations (not shown).

13 The combination of the information from the composite meteorological maps (Figs 2-4) and the HYSPLIT back-
14 trajectories for the April episode (Fig. 10) shows that the prevailing NW wind during the days preceding the
15 episode passed over the N. Atlantic region, where the IASI satellite detects a high ozone area extended
16 throughout the whole troposphere (Figs 5, 6), which beyond any doubt contributes to the high surface ozone
17 values. So, tropospheric transport of air rich in ozone from northern directions is likely to give an important
18 contribution to the high surface ozone levels through the processes of advection and subsidence.

19 It should be noticed at this point that the interpretation of the back trajectory information is much more efficient
20 if it is done in combination with the examination of the composite meteorological charts (and ideally satellite
21 ozone measurements and modelling simulations). In this way the influence from areas with strong tropospheric
22 subsidence and low atmospheric humidity (indicating high ozone) at the various tropospheric pressure levels
23 could be easier assessed.

24 In summary, the April 26-27, 2008 ozone episode could be considered as a clear case of the tropospheric
25 influence to the boundary layer through ozone transport, which is added to the photochemically produced
26 boundary layer ozone. The analysis of meteorological charts at various tropospheric pressure levels helps in
27 understanding that the strong subsidence occurring over the central Mediterranean plays a key role in explaining
28 this surface ozone episode on April 26-27, 2008. The IASI observations of lower and upper tropospheric ozone,
29 helps in understanding that the subsidence of ozone-rich air masses characterizes this surface ozone episode. The
30 evolution of the above described phenomenon can be effectively monitored by examining the composite
31 meteorological maps at 850hPa during the episode days (as well as at 5-days, 3-days and 2-days before the
32 episode). As mentioned, the examination of the 700hPa and 500hPa pressure levels (not shown) gives
33 comparable results.

34 Based on the above results, the simultaneous strengthening and expansion of the African anticyclone and the
35 formation of a cut-off low over the SE Balkans during the episode seem to give rise to the large scale subsidence,
36 inducing a strong downward transport of cold air masses over the western Mediterranean and the surrounding
37 areas while the maximum intensity of the phenomenon is observed in the geographical area located between the
38 two synoptic atmospheric systems. As mentioned, the signs of stronger tropospheric subsidence during the



1 episode days can be clearly observed from the negative specific humidity anomalies as well as the negative
2 columnar precipitable water anomalies associated with positive omega anomalies (downward motion). The
3 evolution of the temperature anomaly is interesting as the growing region of negative temperature anomaly over
4 more or less the region of subsidence (mostly to its west) as the episode develops, could be explained by the
5 descend of much colder air from the upper tropospheric layers caused by the interaction of the low pressure
6 system (located to the east) and the anticyclone (located to the west). This is also consistent with the descent of
7 upper tropospheric tracers simulated with the CHIMERE model. All the above features accompanying a situation
8 with deep subsidence appear in all examined pressure levels at 850 hPa, 700hPa and 500 hPa.

9

10 **3.3 Geographical distribution of meteorological parameters, IASI tropospheric ozone measurements and** 11 **CHIMERE modelling tracer simulations during the May 7-9, 2008 ozone episode**

12 As it will be shown in the next paragraphs, the examination of the May 7-9, 2008 episode leads to comparable
13 remarks regarding synoptic meteorology and geographical distribution of meteorological parameters with the
14 April episode, although in the May episode the meteorological systems and especially the anticyclone are located
15 further to the north. In Figures 11, 12 and 13 the composite NCEP/NCAR Reanalysis maps for the high ozone
16 episode of May 7-9, 2008 at 850 hPa as well as for 2, 3 and 5 days before are presented while the same plots for
17 the 700 hPa, 500 hPa and 300 hPa level have been also created (not shown). Their examination gives the
18 following:

19 a). A deep and extended low is located over N. Atlantic while a strong anticyclone prevails over N. Europe,
20 centered between Great Britain and Scandinavia. At the same time deep and extended low-pressure systems over
21 the polar regions and E. Europe are formed, associated with very dry conditions observed throughout the whole
22 troposphere (Fig. 11).

23 b). Over a part of the anticyclonic area and especially at the region of interface of the anticyclone with the low
24 pressure systems to the east (Fig. 12), an extended area of positive vertical velocity omega (and anomalies) is
25 observed, associated also with extended areas of low-humidity air masses (Fig. 11), which are clear signs of
26 strong subsidence lasting for many days. The signs of subsidence are particularly strong also at the higher
27 tropospheric pressure levels up to 300hPa (not shown) indicating the occurrence of a large-scale tropospheric
28 phenomenon.

29 c). A strong contrast is observed (Fig. 13) between positive and negative temperature anomalies in W. and E.
30 Europe respectively (and also geopotential height anomalies, not shown), which is similar to what has been
31 observed for the April episode, showing strong influence of vertical transport of air masses which tends to occur
32 at the interface areas between high and low atmospheric pressures systems as well as between the associated
33 positive and negative temperature anomalies.

34 d). Stagnant conditions are observed at the center of the N. European anticyclone located over the North Sea
35 while at the southern part of the anticyclone a strong positive vertical omega velocity is observed (indicating
36 subsidence), which is associated with a stronger vector wind velocity over C. Europe. In fact, a strong air current



1 starting from the N. Atlantic makes a circular clockwise motion at the periphery of the anticyclone towards the
2 East while the flow at the northern and the western periphery of the anticyclone is particularly strengthened (Fig.
3 13). Similar features are also observed at the higher pressure levels (700hPa, 500 hPa and 300hPa) as it was also
4 the case for the April episode.

5 In Figure 14, the IASI measurements (composite charts) during the May 7-9, 2008 episode for the lower and the
6 upper troposphere (3 and 10km respectively) as well as for the previous 2, 3 and 5 days are shown. During the
7 May episode a high ozone area is observed in the lower and upper troposphere over the N. Atlantic, which is
8 more extended during the days preceding the episode peak.

9 As observed in Figure 14, the days before the episode and over the region covered by the anticyclone, the
10 concentrations of ozone in the upper troposphere (at 10 km) decrease, while the IASI measurements in the lower
11 troposphere (at 3 km) over central Europe show a small but geographically extended increase. It has to be
12 reminded that this phenomenon takes place exactly over the area where intense subsidence and low humidity
13 conditions have been detected, which could be considered as a direct independent evidence of the influence of
14 ozone concentrations from the upper troposphere, as it has been described and discussed in the previous
15 paragraphs. As also seen in Figure 14, over E. Europe and Russia a significant tropospheric ozone accumulation
16 occurs while a prevailing easterly flow from these high ozone areas is moving towards central and W. Europe
17 (Fig. 13). It should be reminded that over central Europe extended strong subsidence associated with dry
18 conditions and a strong gradient of temperature anomalies are observed at the same time (Figs 11-13).

19 The above features are more clearly shown in Fig. 15 where the daily IASI satellite ozone measurements at 3 and
20 10 km level for the May 2008 episode are presented in a higher concentration resolution as well as in a more
21 restricted geographical domain (same as the CHIMERE model outputs) while the corresponding daily
22 meteorological charts of columnar precipitable water anomaly and geopotential heights at 500hPa and 700hPa
23 are shown in Fig. 16. In fact, an extended region of negative columnar precipitable water anomalies (dry
24 conditions throughout the troposphere, indicating subsidence), prevailing over a vast area covering eastern and
25 central Europe is observed. As also seen in the April episode, this feature appears at the interface areas of the
26 high and low pressure systems while the same synoptic patterns occur at all examined tropospheric levels.

27 The results of the CHIMERE simulations for the May episode are shown in Fig. 17-18, where simulations of
28 upper tropospheric tracer concentrations, simulations of photochemical production and simulations of the ozone
29 field (together with the iso-contours of the high tropospheric tracer) are presented. As described earlier (cf
30 Chapter 2), we use one tracer initialized within the model top layer in the upper troposphere at about 11 km
31 height. Inspecting qualitatively simulated concentrations at 3 km and 1.5 km altitude (Fig. 17, 18), it appears that
32 the upper tropospheric tracer is clearly detected at these levels, indicating downward transport from the upper
33 troposphere to the boundary layer. Also in Fig. 18, the CHIMERE simulations of the ozone fields at 3 km and
34 1.5 km altitudes (corresponding to 700hPa and 850hPa pressure levels respectively) show high ozone
35 concentrations over C. Europe, Italy and the W. Mediterranean. More precisely, the highest upper tropospheric
36 tracer influence occurs to the south of the N. European anticyclone and it is progressively strengthened between
37 7 and 9 of May while high ozone is observed over the whole anticyclonic area. In general, over that area the
38 observed high values of the upper tropospheric tracer indicate considerable subsidence at 5 km altitude (not



1 shown), which becomes even stronger and more extended at the at 3 km and 1.5 km altitudes (Fig. 18).
2 Therefore, the downward transport of upper tropospheric ozone is influencing the lower troposphere and the
3 boundary layer over the examined location. The observed patterns, based on CHIMERE tracer simulations are
4 quite consistent with the above described analysis based on meteorological charts (Figs 11-13) and IASI satellite
5 measurements (Figs 14, 15).

6 Regarding the comparison of the CHIMERE ozone field at 3 km with IASI at 700hPa there is in general a good
7 agreement over Italy and the central Mediterranean but there are differences in E. Europe (lower CHIMERE
8 values) and N. Europe (higher CHIMERE values), which might imply an underestimation of tropospheric
9 transport in E. Europe or overestimation of photochemistry in N. Europe. It should be reminded that similar
10 features appear also in the April episode, described previously. Nevertheless, as mentioned also for the April
11 episode, it should be kept in mind that for a direct quantitative comparison between CHIMERE and IASI data,
12 an application of IASI averaging kernels (smoothing functions) to CHIMERE output would be required
13 (Eremenko et al., 2008).

14 The graphical representation on the map of the daily evolution of the hourly surface ozone concentrations at
15 15:00 h as recorded in the air pollution stations of the EEA-AirBase network (EEA, 2015) during the 7-9 May
16 period (Fig. 18) shows very high concentrations, exceeding 70 ppb, appearing simultaneously at many locations
17 from N. Italy to the British islands. This is in a very good agreement with the CHIMERE tracer simulations as
18 well as the composite meteorological maps (Figs 11-13, 16) and the IASI satellite measurements (Figs 14-15),
19 showing an extended region of subsiding dry air masses over eastern and central Europe. As mentioned
20 previously, during the afternoon hours the influence of the free troposphere on the boundary layer is maximized
21 through vertical mixing and thus the surface ozone concentrations could be increased by the entrainment of
22 subsiding ozone-rich air.

23 In Figure 19 the HYSPLIT back-trajectories during the episode at EMEP stations in Italy (IT04) and France
24 (FR10, FR14) show subsiding air masses arriving either from the north after performing a circular clockwise
25 movement or from the NE (E. Europe and Russia) where high tropospheric ozone concentrations have been
26 recorded by IASI (Figs. 14-15). This is an additional confirmation that air masses originating from areas with
27 high tropospheric ozone concentrations transport ozone down to the ground, leading to high surface ozone
28 values.

29

30 **3.3.1 Ozone vertical profiles over Payerne, Uccle and Hohenpeissenberg during the May 2008 ozone** 31 **episode**

32 Due to the more complex nature of the May 7-9, 2008 ozone episode, the vertical ozone profiles at three
33 European ozone sounding stations (Payerne-Switzerland, Hohenpeissenberg-Germany and Uccle-Belgium) were
34 taken into account for the analysis and the respective vertical ozone measurements for each station are shown in
35 Fig 20.

36 It has to be reminded that the Payerne site is one of the two Swiss stations, where the rural afternoon surface
37 ozone values during the May episode were about 75 ppb (Figs 1-2). The composite meteorological maps (Figs



1 11-13) indicate that the Payerne site was within the area influenced by subsidence. As observed in Fig. 20 a
2 layer with the tropospheric ozone maximum concentration and low relative humidity is at the beginning of the
3 event (on May 5) located between 5 and 6 km altitude. On May 7 a similar layer is seen at a somewhat lower
4 altitude and on May 9 the tropospheric ozone maximum is found below 2000 m altitude. It has to be added that
5 on May 12, at the end of the episode, the vertical ozone profile has changed completely and the ozone
6 concentrations up to 6 km were about 60 ppb (not shown). As mentioned in the meteorological analysis of the
7 episode (Figs 11-13), the downward ozone transport from the ozone-rich lower troposphere to the boundary
8 layer during the 5-9 May period with strong and persistent subsidence, is reflected clearly in the ozone profiles
9 over Payerne (Fig. 18). Based on the observed conditions the plausible explanation is that an “ozone fumigation”
10 of the boundary layer occurred between 5-9 May when the ozone levels increased by at least 20 ppb, following
11 corresponding changes in the lower troposphere and indicating that this ozone event is related to downward
12 transport of ozone from higher altitudes towards the boundary layer.

13 Similar observations could be made at Hohenpeissenberg and Uccle during the May 5-9 period (Fig. 20) where
14 high ozone layers are also observed in the lower troposphere (around 80 – 100 ppb at 3-5 km on May 5 over both
15 sites) and which clearly move downwards. The observed pattern is in agreement with the strong and persistent
16 subsidence observed over the area during the examined days, as it was the case for Payerne. As shown in the
17 vertical ozone soundings (Fig. 20) the high ozone tongue in the troposphere is going down rapidly at a 1-2 km
18 /day rate. At the same time over the examined area the positive vertical velocity omega (and anomalies)
19 observed are associated with dry air (Figs 11-13), indicating subsidence from the upper troposphere all the way
20 down to the surface.

21 It has to be noticed at this point that vertical ozone profiles over the airports of Frankfurt and London carried out
22 in the framework of the MOZAIC project (Marengo et al., 1998; Thouret et al., 2006) during the examined
23 period show almost exactly the same picture (not shown).

24

25 Taking into account all the above information regarding the May episode, the following remarks regarding the
26 tropospheric ozone distribution could be made:

27 a). The IASI satellite measurements shows that over N. Atlantic and to the west of the N. European anticyclone
28 (present at all tropospheric pressure levels up to 300hPa) there are high amounts of ozone in the upper and lower
29 troposphere.

30 b). The anticyclone transports these air masses from the west to the east in a clockwise rotating movement.

31 c). Over E. Europe and at the southern part of the anticyclone the air masses show strong signs of subsidence
32 (downward vertical velocities, dry air), which is particularly enhanced in the vicinity of the strong low-pressure
33 system over eastern Europe.

34 d). A significant ozone decrease in the upper troposphere is observed over the region covered by the N.
35 European anticyclone followed by a slight but extended ozone increase in the lower troposphere, located over the
36 area with intense subsidence (Central Europe) to the south of the anticyclone, with a several day time-shift.



1 In summarizing the observations on the May 7-9, 2008 episode an important question is to which extent the high
2 surface ozone levels observed at first in countries surrounding the western Mediterranean basin but also over a
3 large area in central Europe are influenced by entrainment of ozone rich air from higher layers of the
4 troposphere. An interesting feature is that during the examined period an extended area of strong and persistent
5 downward movement of air masses is observed over Central Europe and lasts for many days. Another important
6 observation is that the wind makes a circular downward motion around the anticyclone while this air current is
7 influenced from regions of very high tropospheric ozone surrounding the anticyclone (located over the observed
8 low pressure systems), according to IASI observations. The high ozone areas coincide very well with extended
9 areas of low humidity as observed in the 850hPa level charts but also at higher tropospheric levels. At the same
10 time, the vertical ozone profiles over Payerne, Uccle and Hohenpeissenberg show concentrations at 60-80 ppb on
11 the top of the boundary layer. It should be noticed that all the above sites are located more or less within the
12 region of high subsidence as the meteorological analysis shows. The CHIMERE tracer simulation experiments
13 are in very good agreement with the above observational analysis. As observed, during this episode the high
14 measured tropospheric ozone background values contribute very significantly, through subsidence, to enhanced
15 ozone values especially over France, Switzerland, northern Italy, and the Western Mediterranean basin, while
16 regional ozone photochemical production is the dominant factor for ozone enhancement over the British Islands,
17 the North Sea as well as on the Iberia peninsula and parts of France (Fig. 17).

18 Summarizing all the above, during the examined May episode as well as in the previous April episode, high
19 atmospheric pressures prevail over the Western Mediterranean and Central Europe while low-pressure systems
20 are observed in Eastern Europe. In general, both examined episodes (26-27 April 2008 and 7-9 May 2008) seem
21 to show comparable characteristics: At first, very strong positive omega anomalies (strong downward air motion
22 or subsidence) are observed over large areas including the Italian peninsula and Central Europe. At the same
23 time, strong negative specific humidity anomalies and negative precipitable water anomalies (indicating dry air
24 in the troposphere) are detected. An interesting feature is that the subsidence area is located at the interface of
25 positive and negative anomalies of geopotential heights and temperature. For the May episode, although the
26 major anticyclone seems to be located away from the Mediterranean basin to the north, a large-scale downward
27 transport towards the Mediterranean according to the meteorological analysis is observed. It comes out from the
28 above analysis that the interpretation of the back trajectory information is much more efficient if it is done in
29 combination with the examination of the meteorological charts (and ideally supported by satellite measurements
30 and modelling simulations), so that the regions with strong subsidence and dry air, are detected and taken into
31 account in the interpretation.

32

33 3.4 Diurnal variation of surface ozone and humidity during the ozone episodes

34 The measurements of surface ozone, relative humidity and temperature at the EMEP site at Ispra, Italy, (Jensen,
35 2016) have been used during the April and May episodes in order to observe the relationship between ozone and
36 absolute humidity (Fig. 21), which could be a good indicator for the detection of the free tropospheric influence
37 to the boundary layer being insensitive to the diurnal temperature variation. Absolute humidity is shown in units
38 of hPa water vapor partial pressure, calculated from the relative humidity using the August-Roche-Magnus



1 formula to find the saturated water vapor partial pressure at the measured temperature. The ozone concentrations
2 show a characteristic diurnal variation with a minimum during the night, followed by a rapid increase in the
3 morning when the nocturnal boundary layer breaks down and air from the above layer reaches the ground. For
4 all days with high ozone during the May episode and for some days during the April episode the ozone increase
5 at mid-day with the maximum vertical mixing is clearly anticorrelated with absolute humidity. This is
6 compatible with the fact that the Ispra site, according to the meteorological analysis presented above, during the
7 whole duration of the May episode is expected to be influenced by subsidence of dry air while during the April
8 episode much stronger anticorrelations and lower absolute humidity levels are observed for some days. Based on
9 the presented example, a first identification of possible direct tropospheric influence to the boundary layer air
10 could be performed at air pollution monitoring stations potentially influenced by tropospheric subsidence.

11

12 **4 Conclusions**

13 In this paper, the investigation of the regional ozone episodes in the western Mediterranean and the surrounding
14 countries is focused on the spring season.

15 Based on the ozone measurements at the EMEP rural ozone stations surrounding the western Mediterranean
16 basin (as well as the EEA-AirBase network), it is observed that episodic periods of high ozone may last for
17 several days and they can be detected at several countries at the same time.

18 An interesting result was that the examined ozone episodes are linked to meteorological conditions very similar
19 to those observed in the eastern Mediterranean (Kalabokas et al., 2013; Doche et al., 2014; Kalabokas et al.,
20 2015), related essentially with transport of ozone-rich tropospheric air masses and the atmospheric subsidence
21 phenomenon. Based on the analysis of the selected springtime ozone episodes, the characteristics associated with
22 high ozone concentrations close to the surface through important subsidence and in connection with high
23 tropospheric ozone levels occurring in the wider area, are the following:

24 The geographic areas with observed deep tropospheric subsidence seem to be the transition regions between a
25 high pressure system, located in the west sector, and a low pressure system located in the east sector, as shown in
26 the corresponding charts of the geopotential heights. Over these areas, strong gradients of geopotential height
27 and temperature are observed together with high omega vertical velocity values and low specific humidity values
28 at the 850hPa as well as at higher tropospheric pressure levels. In addition, over the areas of deep tropospheric
29 subsidence, negative temperature anomalies are observed at these levels and also high vector wind speeds, which
30 means that subsidence is associated with strong advection. The above observational analysis is in very good
31 agreement with IASI satellite measurements and CHIMERE tracer simulation experiments.

32 The present approach, using meteorological charts, IASI tropospheric ozone satellite measurements, CHIMERE
33 tracer simulations and back trajectories for the analysis of selected spring ozone episodes, shows to be quite
34 efficient in the analysis of atmospheric conditions and transport patterns associated with the episodes, which
35 need to be adequately described in numerical chemical-transport models used for simulations of air pollution. It
36 can be useful for the study of the tropospheric influence on the boundary layer and the ground surface, especially
37 for tracing large scale deep subsidence events (downward movements of generally dry air masses) when



1 analyzing surface (and vertical, if available) measurements at sites in the Mediterranean basin, where this
2 phenomenon is quite frequent, and also in other places worldwide. For example, similar field observations on the
3 influence of upper atmospheric layers on the boundary layer and surface measurements have been reported at
4 some locations in the United States (Parrish et al., 2010; Cooper et al., 2011; Langford et al., 2015). In addition,
5 the consideration for the analysis of ozone measurements presented above is in agreement with recent
6 observations in Atlantic and European regions indicating significant tropospheric (and even stratospheric)
7 influence to the surface and boundary layer ozone measurements (Trickl et al., 2010; Trickl et al., 2011; Logan
8 et al., 2012; Cuevas et al., 2013; Hess and Zbinden, 2013; Cooper et al., 2014; Parrish et al., 2014).

9 Regarding the environmental policy issues, it has to be underlined that for ozone, which is a pollutant regulated
10 by the EU, it appears that there are some time periods during the warm period of the year, lasting for several
11 days, when the free troposphere influences significantly the boundary layer to such extent that the air quality
12 standards might be exceeded. This phenomenon seems to be associated with an important impact of
13 photochemical ozone production following primary air pollutant emission at larger geographical scales,
14 including transport of air pollutants on a hemispheric scale from e.g. the US and China. The origin of the
15 atmospheric ozone entering the boundary layer might be upper tropospheric or stratospheric but it could also be
16 from the lower or the middle troposphere during stagnant regional conditions when photochemical ozone is
17 produced over the continent.

18 Further detailed and quantitative studies of this phenomenon appear to be needed to improve our understanding
19 of the mechanisms associated with intercontinental pollution as well as regional photochemical pollution could
20 be improved, already highlighted by the work of the HTAP (Hemispheric Transport of Air Pollution) project.
21 The Mediterranean region which seems to be mostly affected is the Eastern Mediterranean, where the 60 ppb EU
22 standard is very frequently exceeded during the warm period of the year and especially during July-August when
23 the atmospheric subsidence is a quite common atmospheric feature and almost quasi-permanent, but as shown in
24 the present study, also in the Western Mediterranean a similar mechanism could be observed, especially during
25 the spring season. The strategies for obtaining compliance with the EU ozone standard may need to be
26 reconsidered by taking into account the contribution from regional and intercontinental transport.

27

28 Acknowledgements

29 The composite weather maps were provided by the NOAA/ESRL Physical Sciences Division, Boulder Colorado
30 from their Web site at <http://www.cdc.noaa.gov/>, which is gratefully acknowledged. The authors also
31 acknowledge the NOAA Air Resources Laboratory (ARL) for the provision of the HYSPLIT transport and
32 dispersion model and/or READY website (<http://www.ready.noaa.gov>) used in this publication. Also, Dr. A.
33 Volz-Thomas, FZ-Juelich, is acknowledged for interesting discussion as well as Dr. C. Repapis, Academy of
34 Athens, for useful comments on the manuscript. JRC is acknowledged for an EU grant (cat. 40) to one of the
35 authors (P. K.).

36

37



1 **References**

- 2 Beekmann, M. and Vautard R., 2010. A modelling study of photochemical regimes over Europe: robustness and
3 variability, *Atmos. Chem. Phys.*, 10, 10067-10084.
- 4 Beekmann, M., Ancellet, G. and Megie, G. 1994. Climatology of tropospheric ozone in southern Europe and its
5 relation to potential vorticity. *J. Geophys. Res.*, 99, 12841-12853.
- 6 Bonasoni, P., Stohl, A., Cristofanelli, P., Calzolari, F., Colombo, T. and Evangelisti, F. 2000. Background ozone
7 variations at Mt. Cimone station. *Atmos. Environ.* 34, 5183-5189.
- 8 Boynard, A., Clerbaux, C., Coheur, P.-F., Hurtmans, D., Turquety, S., George, M., Hadji-Lazaro, J., Keim, C.,
9 and Meyer-Arnek, J. 2009. Measurements of total and tropospheric ozone from IASI: comparison with
10 correlative satellite, ground-based and ozonesonde observations, *Atmos. Chem. Phys.*, 9, 6255–6271,
11 doi:10.5194/acp-9-6255-2009.
- 12 Clarisse, L., R'Honi, Y., Coheur, P.-F., Hurtmans, D., and Clerbaux, C., 2011. Thermal infrared nadir
13 observations of 24 atmospheric gases, *Geophys. Res. Lett.*, 38, L10802, doi:10.1029/2011GL047271.
- 14 Clerbaux, C., Boynard, A., Clarisse, L., George, M., Hadji-Lazaro, J., Herbin, H., Hurtmans, D., Pommier, M.,
15 Razavi, A., Turquety, S., Wespes, C., and Coheur, P.-F. 2009. Monitoring of atmospheric composition using the
16 thermal infrared IASI/MetOp sounder, *Atmos. Chem. Phys.*, 9, 6041–6054, doi:10.5194/acp-9-6041-2009.
- 17 Coheur, P.-F., Barret, B., Turquety, S., Hurtmans, D., Hadji-Lazaro, J., and Clerbaux, C. 2005. Retrieval and
18 characterization of ozone vertical profiles from a thermal infrared nadir sounder, *J. Geophys. Res.*, 110, D24303,
19 doi:10.1029/2005JD005845.
- 20 Cooper, O.R., Oltmans, S.J., Johnson, B.J., Brioude, J., Angevine, W., Trainer, M., Parrish, D. D., Ryerson, T.
21 R., Pollack, I., Cullis, P. D., Ives, M.,A., Tarasick D.W., Al-Saadi, J., Stajner, I. 2011. Measurement of western
22 U.S. baseline ozone from the surface to the tropopause and assessment of downwind impact regions. *J. Geophys.*
23 *Res* 116:D00V03. doi:10.1029/2011JD016095
- 24 Cooper, O. R., Gao, R.-S., Tarasick, D., Leblanc, T., Sweeney, C. 2012. Long-term ozone trends at rural ozone
25 monitoring sites across the United States, 1990–2010. *J. Geophys. Res* 117: D22307.
26 doi:10.1029/2012JD018261
- 27 Cooper, O. R., Parrish, D. D., Ziemke, J., Balashov, N. V., Cupeiro, M., Galbally, I. E., Gilge, S., Horowitz,
28 L., Jensen, N. R., Lamarque, J.-F., Naik, V., Oltmans, S. J., Schwab, J., Shindell, D. T., Thompson, A. M.,
29 Thouret, V., Wang, Y., Zbinden, R. M. 2014. Global distribution and trends of tropospheric ozone: An
30 observation-based review. *Elementa: Sci. of the Anthropocene*. 2: 000029, doi:
31 10.12952/journal.elementa.000029
- 32 Coman, A., Foret, G., Beekmann, M., Eremenko, M., Dufour, G., Gaubert, B., Ung, A., Schmechtig, C., Flaud,
33 J.-M., and Bergametti, G. 2012. Assimilation of IASI partial tropospheric columns with an Ensemble Kalman
34 Filter over Europe, *Atmos. Chem. Phys.*, 12, 2513–2532, doi:10.5194/acp-12-2513-2012.



- 1 Cristofanelli, P., Scheel, H.-E., Steinbacher, M., Saliba, M., Azzopardi, F., Ellul, R., Froehlich, M., Tositti, L.,
2 Brattich, E., Maione, M., Calzolari, F., Duchi, R., Landi, T.C., Marinoni, A. and Bonasoni P. 2015. Long-term
3 surface ozone variability at Mt. Cimone WMO/GAW global station (2165 m a.s.l., Italy). *Atmos. Environ.* 101,
4 23-33.
- 5 Cuevas, E., González, Y., Rodríguez, S., Guerra, J.C., Gómez-Peláez, A.J., Alonso Pérez, S., Bustos, J., Milford,
6 C. 2013. Assessment of atmospheric processes driving ozone variations in the subtropical North Atlantic free
7 troposphere, *Atmos. Chem. Phys* 13:1973–1998.
- 8 Delmas, R., Mégie, G., and Peuch, V.-H. 2005. *Physique et chimie de l’atmosphère*, Ed. Belin, Coll. Echelles,
9 640
- 10 Doche, C., Dufour, G., Foret, G., Eremenko, M., Cuesta, J., Beekmann, M., and Kalabokas, P. 2014.
11 Summertime tropospheric-ozone variability over the Mediterranean basin observed with IASI, *Atmos. Chem.*
12 *Phys.*, 14, 10589–10600.
- 13 Draxler, R.R. and Rolph, G.D. 2015. HYSPLIT (HYbrid Single-Particle Lagrangian Integrated Trajectory)
14 Model access via NOAA ARL READY Website (<http://www.arl.noaa.gov/HYSPLIT.php>). NOAA Air
15 Resources Laboratory, College Park, MD.
- 16 EEA, 2015: <http://www.eea.europa.eu/themes/air/air-quality/map/airbase>
- 17 Dufour, G., Eremenko, M., Orphal, J., and Flaud, J.-M. 2010. IASI observations of seasonal and day-to-day
18 variations of tropospheric ozone over three highly populated areas of China: Beijing, Shanghai, and Hong Kong,
19 *Atmos. Chem. Phys.*, 10, 3787–3801, doi:10.5194/acp-10-3787-2010.
- 20 Dufour, G., Eremenko, M., Griesfeller, A., Barret, B., LeFlochmoën, E., Clerbaux, C., Hadji-Lazaro, J., Coheur,
21 P.-F. and Hurtmans D., Validation of three scientific ozone products retrieved from IASI spectra using
22 ozonesondes, *Atmos. Meas. Tech.*, 5, 611-630, 2012.
- 23 Dufour, G., Eremenko, M., Cuesta, J., Doche, C., Foret, G., Beekmann, M., Cheiney, A., Wang, Y., Cai, Z., Liu,
24 Y., Takigawa, M., Kanaya, Y., and Flaud, J.-M.: Springtime daily variations in lower-tropospheric ozone over
25 east Asia: the role of cyclonic activity and pollution as observed from space with IASI, *Atmos. Chem. Phys.*, 15,
26 10839-10856, doi:10.5194/acp-15-10839-2015, 2015.
- 27 Eremenko, M., Dufour, G., Foret, G., Keim, C., Orphal, J., Beekmann, M., Bergametti, G., and Flaud, J.-M.
28 2008. Tropospheric ozone distributions over Europe during the heat wave in July 2007 observed from infrared
29 nadir spectra recorded by IASI, *Geophys. Res. Lett.*, 35, L18805, doi:10.1029/2008GL034803.
- 30 Fishman, J., Wozniak, A. E., and Creilson, J. K. 2003. Global distribution of tropospheric ozone from satellite
31 measurements using the empirically corrected tropospheric ozone residual technique: Identification of the
32 regional aspects of air pollution, *Atmos. Chem. Phys.*, 3, 893–907, doi:10.5194/acp-3-893-2003.
- 33 Foret, G., Hamaoui, L., Schmechtig, C., Eremenko, M., Keim, C., Dufour, G., Boynard, A., Coman, A., Ung, A.,
34 and Beekmann, M. 2009. Evaluating the potential of IASI ozone observations to constrain simulated surface
35 ozone concentrations, *Atmos. Chem. Phys.*, 9, 8479–8491, doi:10.5194/acp-9-8479-2009.



- 1 Fuhrer, J. 2009. Ozone risk for crops and pastures in present and future climates, *Naturwissenschaften*, 96, 173–
2 194.
- 3 Hess, P.G., Zbinden, R., 2013. Stratospheric impact on tropospheric ozone variability and trends: 1990–2009,
4 *Atmos. Chem. Phys.*, 13, 649–674.
- 5 George, M., Clerbaux, C., Hurtmans, D., Turquety, S., Coheur, P.-F., Pommier, M., Hadji-Lazaro, J., Edwards,
6 D. P., Worden, H., Luo, M., Rinsland, C., and McMillan, W. 2009. Carbon monoxide distributions from the
7 IASI/METOP mission: evaluation with other space-borne remote sensors, *Atmos. Chem. Phys.*, 9, 8317–8330,
8 doi:10.5194/acp-9-8317-2009.
- 9 Gerasopoulos, E., Kouvarakis, G., Vrekoussis, M., Kanakidou, M., Mihalopoulos, N., 2005. Ozone variability in
10 the marine boundary layer of the Eastern Mediterranean based on 7-year
11 Observations, *J. Geoph. Res.*, 110, D15309.
- 12 Guenther, A., Karl, T., Harley, P., Wiedinmyer, C., Palmer, P. I., and Geron, C. 2006. Estimates of global
13 terrestrial isoprene emissions using MEGAN (Model of Emissions of Gases and Aerosols from Nature). *Atmos.*
14 *Chem. Phys.*, 6, 3181–3210, www.atmos-chem-phys.net/6/3181/2006/
- 15 HTAP report, 2010. Hemispheric Transport of Air Pollution 2010. Part A: Ozone and Particulate Matter, Air
16 Pollution Studies No 17, United Nations Economic Commission for Europe, ISBN 978-92-1-117043-6
- 17 IPCC: Climate Change 2007: The Physical Science Basis, Contribution of Working Group I to the Fourth
18 Assessment Report of the Intergovernmental Panel on Climate Change, edited by: Solomon, S., Qin, D.,
19 Manning, M., Chen, Z., Marquis, M., Averyt, K. B., Tignor, M., and Miller, H. L., Cambridge University Press,
20 Cambridge, United Kingdom and New York, NY, USA, 2007.
- 21 Johnson, J. E., Sundet, J. K., and Tarrason, L. 2001. Model calculations of present and future levels of ozone and
22 ozone precursors with a global and regional model, *Atmos. Environ.*, 35, 525–537.
- 23 Jensen, N.R. (2016), personal communication.
- 24 Kalabokas, P. D., Viras, L. G., Bartzis, J. G., and Repapis, C. C. 2000. Mediterranean rural ozone characteristics
25 around the urban area of Athens, *Atmosph. Environ.*, 34, 5199–5208.
- 26 Kalabokas, P. D. and Repapis, C. C. 2004. A climatological study of rural surface ozone in central Greece,
27 *Atmos. Chem. Phys.*, 4, 1139–1147, doi:10.5194/acp-4-1139-2004.
- 28 Kalabokas, P. D., Volz-Thomas, A., Brioude, J., Thouret, V., Cammas, J.-P., and Repapis, C. C. 2007. Vertical
29 ozone measurements in the troposphere over the Eastern Mediterranean and comparison with Central Europe,
30 *Atmos. Chem. Phys.*, 7, 3783–3790, doi:10.5194/acp-7-3783-2007.
- 31 Kalabokas, P. D., Mihalopoulos, N., Ellul, R., Kleanthous, S., and Repapis, C. C. 2008. An investigation of the
32 meteorological and photochemical factors influencing the background rural and marine surface ozone levels in
33 the Central and Eastern Mediterranean, *Atmos. Environ.*, 42, 7894–7906
- 34 Kalabokas, P. D., Cammas, J.-P., Thouret, V., Volz-Thomas, A., Boulanger, D., and Repapis, C. C. 2013.
35 Examination of the atmospheric conditions associated with high and low summer ozone levels in the lower



- 1 troposphere over the eastern Mediterranean, Atmos. Chem. Phys., 13, 10339–10352, doi:10.5194/acp-13-10339-
2 2013.
- 3 Kalabokas, P. D., Thouret, V., Cammas, J.-P., Volz-Thomas, A., Boulanger, D., and Repapis, C. C. 2015. The
4 geographical distribution of meteorological parameters associated with high and low summer ozone levels in the
5 lower troposphere and the boundary layer over the Eastern Mediterranean (Cairo case). *Tellus B*, 67, 27853,
6 <http://dx.doi.org/10.3402/tellusb.v67.27853>
- 7 Kalnay, E., Kanamitsu, M., Kistler, R., Collins, W., Deaven, D., Gandin, L., Iredell, M., Saha, S., White, G.,
8 Woolen, J., Zhu, Y., Chelliah, M., Ebisuzaki, W., Higgins, W., Janowiak, J., Mo, K. C., Ropelewski, C., Wang,
9 J., Leetmaa, A., Reynolds, R., Jenne, R., and Joseph, D. 1996. The NCEP/NCAR Reanalysis 40-year Project, *B.*
10 *Am. Meteorol. Soc.*, 77, 437–471.
- 11 Kleanthous, S., Vrekoussis, M., Mihalopoulos, N., Kalabokas, P. and Lelieveld, J. 2014. On the temporal and
12 spatial variation of ozone in Cyprus. *Sc. of the Tot. Environ.* 476–477 (2014), 677–687.
- 13 Kourtidis, K., Zerefos, C., Rapsomanikis, S., Simeonov, V., Balis, D., Perros, P. E., Thomson, A. M., Witte, J.,
14 Calpini, B., Sharobiem, W. M., Papayiannis, A., Mihalopoulos, N., and Drakou, R. 2002. Regional levels of
15 ozone in the troposphere over eastern Mediterranean, *J. Geophys. Res.*, 107, 8140, doi:10.1029/2000JD000140.
- 16 Kouvarakis, G., Vrekoussis, M., Mihalopoulos, N., Kourtidis, K., Rappenglueck, B., Gerasopoulos, E., and
17 Zerefos, C. 2002. Spatial and temporal variability of tropospheric ozone in the boundary layer above the Aegean
18 Sea (eastern Mediterranean), *J. Geophys. Res.*, 107, 8137, doi:10.1029/2000JD000081.
- 19 Kuenen, J. J. P., Visschedijk, A. J. H., Jozwicka, M. and Denier van der Gon, H. A. C. 2014. TNO-MACC_II
20 emission inventory; a multi-year (2003–2009) consistent high-resolution European emission inventory for air
21 quality modeling, *Atmos. Chem. Phys.*, 14, 10963–10976, doi:10.5194/acp-14-10963-2014, 2014.
- 22 Langford, A.O., Sen, C.J., Alvarez, R.J., Brioude, J., Cooper, O.R., Holloway, J.S., Lind, M.Y., Marchbanksa,
23 R.D., Pierce, R.B., Sandberg, S.P., Weickmann, A.M., Williams, E.J. 2015. An Overview of the 2013 Las
24 Vegas Ozone Study (LVOS): Impact of stratospheric intrusions and long-range transport on surface air quality.
25 *Atmos. Environ.*, 109, 305–322.
- 26 Levy, J. I., Carrothers, T. J., Tuomisto, J. T., Hammitt, J. K., and Evans, J. S. 2001. Assessing the Public Health
27 Benefits of Reduced Ozone Concentrations, *Environ. Health Perspect.*, 109, 1215– 1226.
- 28 Lelieveld, J., Berresheim, H., Borrmann, S., Crutzen, P. J., Dentener, F. J., Fischer, H., Feichter, J., Flatau, P. J.,
29 Heland, J., Holzinger, R., Korrman, R., Lawrence, M. G., Levin, Z., Markowicz, K. M., Mihalopoulos, N.,
30 Minikin, A., Ramanathan, V., de Reus, M., Roelofs, G. J., Scheeren, H. A., Sciare, J., Schlager, H., Schultz, M.,
31 Siegmund, P., Steil, B., Stephanou, E. G., Stier, P., Traub, M., Warneke, C., Williams, J., and Ziereis, H. 2002.
32 Global air pollution crossroads over the Mediterranean, *Science*, 298, 794–799.
- 33 Lelieveld, J. 2009. Air pollution and climate, in: *The Physical Geography of the Mediterranean*, edited by:
34 Woodward, J. C., Oxford University Press, 599–614.



- 1 Li, Q., Jacob, D. J., Logan, J. A., Bey, I., Yantosca, R. M., Liu, H., Martin, R. V., Fiore, A. M., Field, B. D.,
2 Duncan, B. N., and Thouret, V. 2001. A tropospheric ozone maximum over the Middle East, *Geophys. Res.*
3 *Letts.*, 28, 3235–3238, doi:10.1029/2001GL013134.
- 4 Liu, X., Chance, K. V., Sioris, C. E., Spurr, R. J. D., Kurosu, T. P., Martin, R. V., and Newchurch, M. J. 2005.
5 Ozone profile and tropospheric ozone retrievals from Global Ozone Monitoring Experiment: Algorithm
6 description and validation, *J. Geophys. Res.*, 110, D20307, doi:10.1029/2005JD006240.
- 7 Liu, J. J., Jones, D. B. A., Worden, J. R., Noone, D., Parrington, M., and Kar, J. 2009. Analysis of the
8 summertime build-up of tropospheric ozone abundances over the Middle East and North Africa as observed by
9 the Tropospheric Emission Spectrometer instrument, *J. Geophys. Res.*, 114, D05304,
10 doi:10.1029/2008JD010993.
- 11 Logan, J. A., Staehelin, J., Megretskaia, I. A., Cammas, J.-P., Thouret, V., Claude, H., De Backer, H.,
12 Steinbacher, M., Scheel, H.-E., Stübi, R., Fröhlich M. and Derwent R. 2012. Changes in ozone over Europe:
13 Analysis of ozone measurements from sondes, regular aircraft (MOZAIC) and alpine surface sites, *J. Geophys.*
14 *Res.*, 117, D09301, doi:10.1029/2011JD016952.
- 15 Marengo, A., Thouret, V., Nédélec, P., Smit, H., Helten, M., Kley, D., Karcher, F., Simon, P., Law, K., Pyle, J.,
16 Poschmann, G., Von Wrede, R., Hume, C., and Cook, T. 1998. Measurements of ozone and water vapor by
17 Airbus in-service aircraft: The MOZAIC airborne program. An overview, *J. Geophys. Res.*, 103, 25631–25642.
- 18 Menut, L., Bessagnet, B., Khvorostyanov, D., Beekmann, M., Blond, N., Colette, A., Coll, I., Curci, G., Foret,
19 G., Hodzic, A., Mailler, S., Meleux, F., Monge, J.-L., Pison, I., Siour, G.,
- 20 Turquety, S., Valari, M., Vautard, R., and Vivanco, M. G. 2013. CHIMERE 2013: a model for regional
21 atmospheric composition modelling, *Geosci. Model Dev.*, 6, 981–1028, doi:10.5194/gmd-6-981-2013.
- 22 Millán, M. M., Salvador, R., Mantilla, E., and Kallos, G. 1997. Photo-oxidant dynamics in the western
23 Mediterranean in summer: Results from European research projects, *J. Geophys. Res.* 102: 8811–23.
- 24 Millan, M.M., Mantilla, E., Salvador, R., Carratalá, R., Sanz, M. J., Alonso, L., Gangioti, G., and Navazo, M.
25 2000. Ozone cycles in the western Mediterranean basin: Interpretation of monitoring data in complex coastal
26 terrain. *J. Appl. Meteor.* 39, 487–508.
- 27 Monks, P. S., 2000. A review of the observations and origins of the spring ozone maximum, *Atmos. Environ.*,
28 34, 3545–3561.
- 29 Monks, P. S., Archibald, A. T., Colette, A., Cooper, O., Coyle, M., Derwent, R., Fowler, D., Granier, C., Law,
30 K. S., Mills, G. E., Stevenson, D. S., Tarasova, O., Thouret, V., von Schneidmesser E., Sommariva, R., Wild,
31 O., and Williams, M. L. 2015. Tropospheric ozone and its precursors from the urban to the global scale from air
32 quality to short-lived climate forcer, *Atmos. Chem. and Phys.*, 15, 8889-8973.
- 33 Nolle, M., Ellul, R., Heinrich, G., and Güsten, H. 2002. A longterm study of background ozone concentrations in
34 the central Mediterranean—diurnal and seasonal variations on the island of Gozo, *Atmospheric Environment* 36:
35 1391–402.



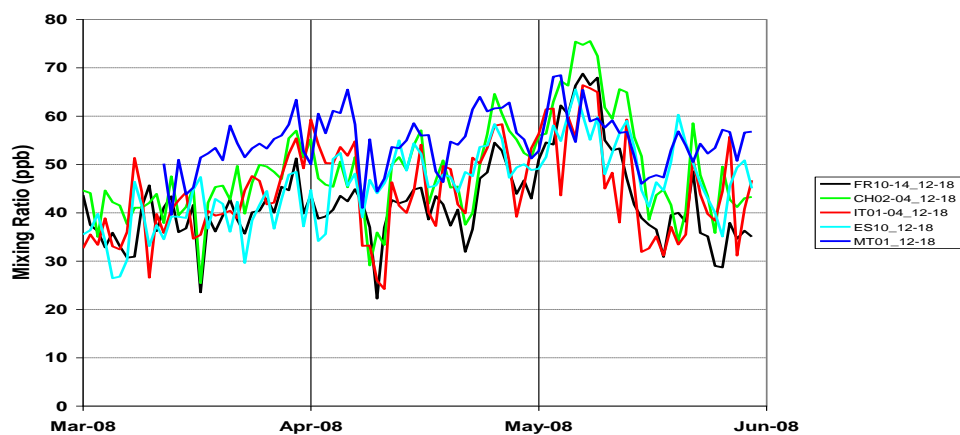
- 1 Paoletti, E. 2006. Impact of ozone on Mediterranean forests: A Review, *Environ. Pollut.*, 144, 463–474.
- 2 Parrish, D. D., Aikin, K. C., Oltmans, S. J., Johnson, B. J., Ives, M., and Sweeny, C. 2010. Impact of transported
3 background ozone inflow on summertime air quality in a California ozone exceedance area, *Atmos. Chem.*
4 *Phys.*, 10, 10093–10109, doi:10.5194/acp-10-10093-2010.
- 5 Parrish, D.D., Law, K.S., Staehelin, J., Derwent, R., Cooper, O.R., Tanimoto, H., Volz-Thomas, A., Gilge, S.,
6 Scheel, H.-E., Steinbacher, M., and Chan, E. 2013. Lower tropospheric ozone at northern mid-latitudes:
7 Changing seasonal cycle. *Geophys. Res. Lett* 40: 1631–1636. doi:10.1002/grl.50303.
- 8 Parrish, D. D., Lamarque, J.-F., Naik, V., Horowitz, L., Shindell, D. T., Staehelin, J., Derwent, R., Cooper, O.
9 R., Tanimoto, H., Volz-Thomas, A., Gilge, S., Scheel, H.-E., Steinbacher, M., and Fröhlich, M. 2014. Long-term
10 changes in lower tropospheric baseline ozone concentrations: Comparing chemistry-climate models and
11 observations at northern midlatitudes, *J. Geophys. Res. Atmos.*, 119, 5719–5736, doi:10.1002/2013JD021435.
- 12 Richards, N. A. D., Arnold, S. R., Chipperfield, M. P., Miles, G., Rap, A., Siddans, R., Monks, S. A., and
13 Hollaway, M. J. 2013. The Mediterranean summertime ozone maximum: global emission sensitivities and
14 radiative impacts, *Atmos. Chem. Phys.*, 13, 2331–2345, doi:10.5194/acp-13-2331-2013.
- 15 Rodwell, M. J. and Hoskins, B. J. 1996. Monsoons and the dynamics of deserts, *Q. J. R. Meteorol. Soc.*, 122,
16 1385–1404, doi:10.1002/qj.49712253408.
- 17 Rodwell, M. J. and Hoskins, B. J. 2001. Subtropical anticyclones and summer monsoons, *J. Climate*, 14, 3192–
18 3211.
- 19 Rouil L., C.Honore, R.Vautard, M.Beekmann, B.Bessagnet, L.Malherbe, F.Meleux, A.Dufour, C.Elichegaray, J-
20 M.Flaud, L.Menut, D.Martin, A.Peuch, V-H.Peuch, N.Poisson, 2009, PREV'AIR : an operational forecasting
21 and mapping system for air quality in Europe, BAMS, DOI: 10.1175/2008BAMS2390.1
- 22 Safieddine, S., Boynard, A., Coheur, P.-F., Hurtmans, D., Pfister, G., Quennehen, B., Thomas, J. L., Raut, J.-C.,
23 Law, K. S., Klimont, Z., Hadji-Lazaro, J., George, M., and Clerbaux C. 2014. Summertime tropospheric ozone
24 assessment over the Mediterranean region using the thermal infrared IASI/MetOp sounder and the WRF-Chem
25 model, *Atmos. Chem. Phys.*, 14, 10119–10131, doi:10.5194/acp-14-10119-2014.
- 26 Sánchez, M. L., García, M. A., Pérez, I. A., and de Torre, B. 2008. Evaluation of surface ozone measurements
27 during 2000–2005 at a rural area in the upper Spanish plateau, *J. Atmos. Chem.*, 60, 137–152.
- 28 Schürmann, G. J., Algieri, A., Hedgecock, I. M., Manna, G., Pirrone, N., and Sprovieri, F. 2009. Modeling local
29 and synoptic scale influences on ozone concentrations in a topographically complex region of Southern Italy,
30 *Atmos. Environ.*, 43, 4424–4434.
- 31 Seinfeld, J. H., Pandis, S. N., 2006. *Atmospheric Chemistry and Physics: From Air Pollution to Climate Change*,
32 2nd Edition, Wiley.
- 33 Sicard, P., De Marco, A., Troussier, F., Renou, C., Vas, N., Paoletti, E. 2013. Decrease in surface ozone
34 concentrations at Mediterranean remote sites and increase in the cities. *Atmos. Environ* 79: 705–715.



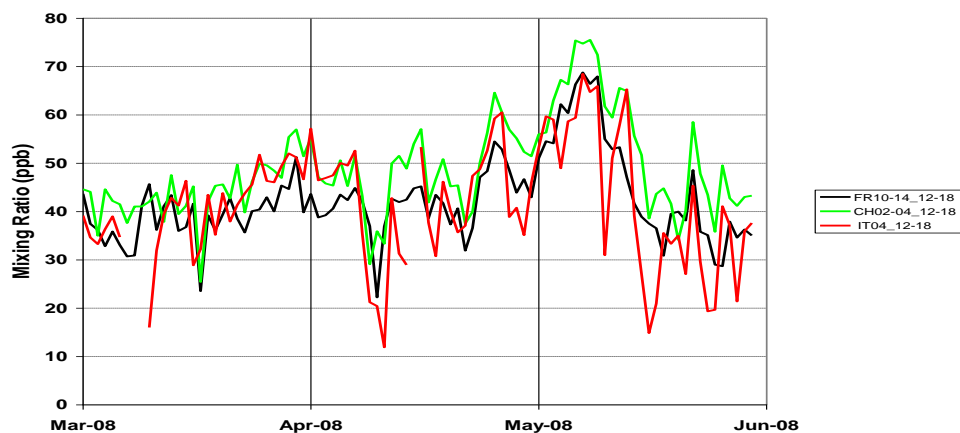
- 1 Stohl, A., Eckhardt, S., Forster, C., James, P., and Spichtinger, N. 2002. On the pathways and timescales of
2 intercontinental air pollution transport, *J. of Geoph. Res(Atm.)*, 107(D23): 4684-4700.
- 3 Thouret, V., Cammas, J.-P., Sauvage, B., Athier, G., Zbinden, R., Nédélec, P., Simon, P., and Karcher, F. 2006.
4 Tropopause referenced ozone climatology and inter-annual variability (1994–2003) from the MOZAIC
5 programme, *Atmos. Chem. Phys.*, 6, 1033–1051, doi:10.5194/acp-6-1033-2006.
- 6 Trickl, T., Feldmann, H., Kanter, H.-J., Scheel, H.-E., Sprenger, M., Stohl, A., and Wernli, H., 2010. Forecasted
7 deep stratospheric intrusions over Central Europe: case studies and climatologies, *Atmos. Chem. Phys.*, 10, 499–
8 524, doi:10.5194/acp-10-499-2010.
- 9 Trickl, T., Bärtsch-Ritter, N., Eisele, H., Furger, M., Mücke, R., Sprenger, M., and Stohl, A. 2011. High-ozone
10 layers in the middle and upper troposphere above Central Europe: potential import from the stratosphere along
11 the subtropical jet stream, *Atmos. Chem. Phys.*, 11, 9343–9366, doi:10.5194/acp-11-9343-2011.
- 12 Tyrlis, E., Lelieveld, J., and Steil, B. 2013. The summer circulation in the eastern Mediterranean and the Middle
13 East: influence of the South Asian Monsoon, *Clim. Dynam.*, 40, 1103–1123, doi:10.1007/s00382-012-1528-4.
- 14 Tyrlis, E., Škerlak, B., Sprenger, M., Wernli, H., Zittis, G., and Lelieveld, J., 2014. On the linkage between the
15 Asian summer monsoon and tropopause fold activity over the eastern Mediterranean and the Middle East, *J.*
16 *Geophys. Res. Atmos.*, 119, 3202–3221, doi:10.1002/2013JD021113.
- 17 Velchev, K., Cavalli, F., Hjorth, J., Marmer, E., Vignati, E., Dentener, F., and Raes, F., 2011. Ozone over the
18 Western Mediterranean Sea – results from two years of shipborne measurements, *Atmos. Chem. Phys.*, 11, 675–
19 688, doi:10.5194/acp-11-675-2011.
- 20 Worden, H. M., Logan, J. A., Worden, J. R., Beer, R., Bowman, K., Clough, S. A., Eldering, A., Fisher, B. M.,
21 Gunson, M. R., Herman, R. L., Kulawik, S. S., Lampel, M. C., Luo, M., Megretskaja, I. A., Osterman, G. B., and
22 Shephard, M.W. 2007. Comparisons of Tropospheric Emission Spectrometer (TES) ozone profiles to ozone-
23 sondes: Methods and initial results, *J. Geophys. Res.*, 112, D03309, doi:10.1029/2006JD007258.
- 24 WOUDC, 2015: <http://woudc.org/data/explore.php>
- 25 Zanis, P., Hadjinicolaou, P., Pozzer, A., Tyrlis, E., Dafka, S., Mihalopoulos, N., and Lelieveld, J. 2014.
26 Summertime free-tropospheric ozone pool over the eastern Mediterranean/Middle East, *Atmos. Chem. Phys.*, 14,
27 115–132, doi:10.5194/acp-14-115-2014.
- 28
- 29



1



2



3

4 **Figure 1: (Upper panel):** Day-to-day variation of the 12:00 - 18:00 afternoon ozone (in $\mu\text{g}/\text{m}^3$) on the
5 EMEP stations surrounding the Western Mediterranean basin for spring 2008: Spain (ES10, light blue),
6 France (FR10-14, black), Switzerland (CH02-04, green), Italy (IT01-04, red), Malta (MT01, blue).

7 **(Lower panel):** Day-to-day variation of the 12:00 - 18:00 afternoon ozone (in $\mu\text{g}/\text{m}^3$) on the EMEP stations
8 close to the Western Mediterranean basin and around the Alpine region for spring 2008: France (FR10-
9 14, black), Switzerland (CH02-04, green), Italy (IT04-JRC, red).

10



1

2

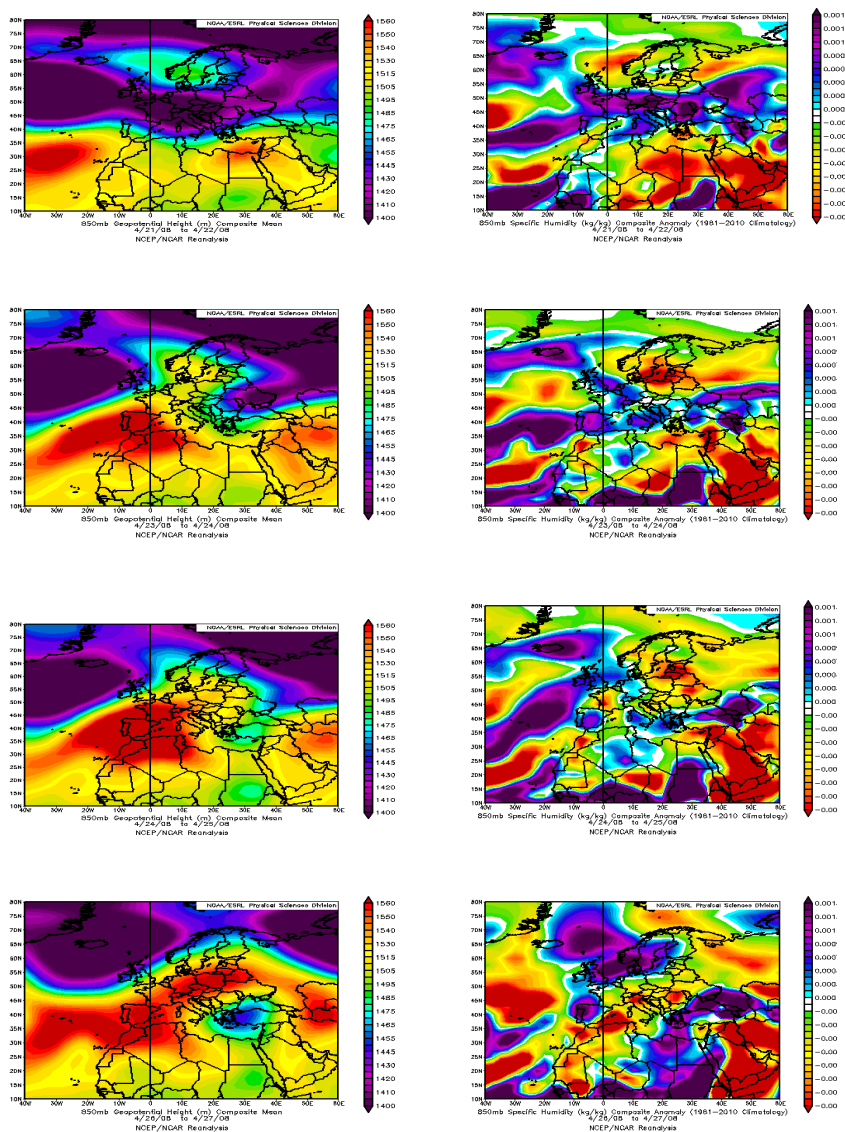
3

4

5

9

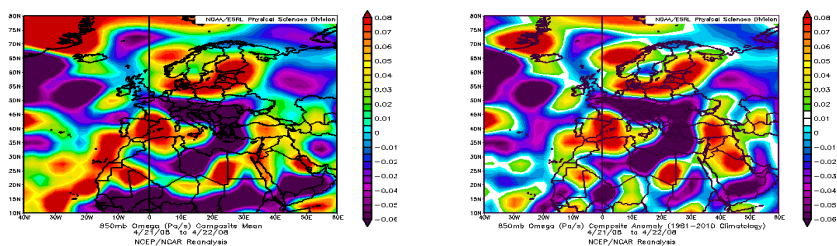
10



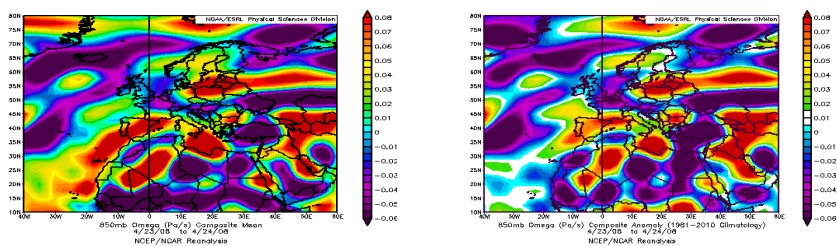
6 **Figure 2: Composite weather maps of geopotential height (left column) and specific humidity (right**
7 **column), for the high ozone episode of 26-27 April 2008 (lowest panels) as well as for two, three and five**
8 **days before.**



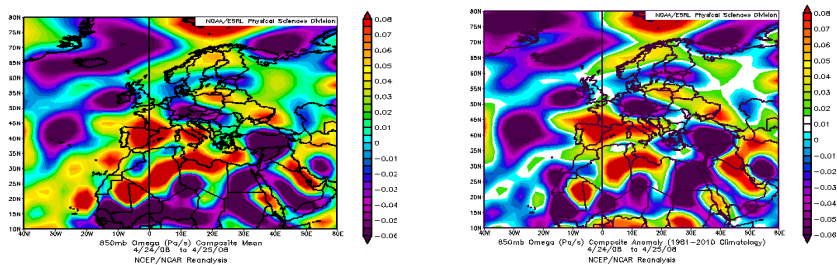
1



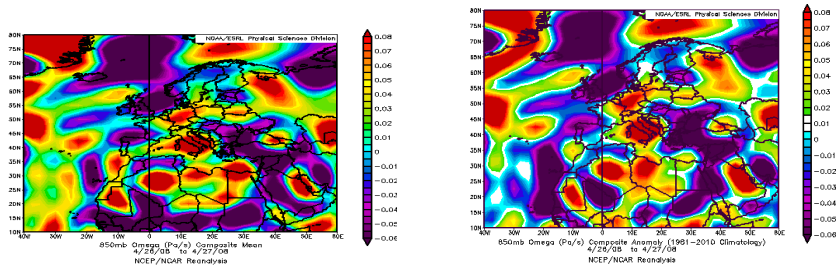
2



3



4



5 **Figure 3: Same as Fig. 2 but for omega vertical velocity (left column) and omega vertical velocity anomaly**
6 **(right column).**

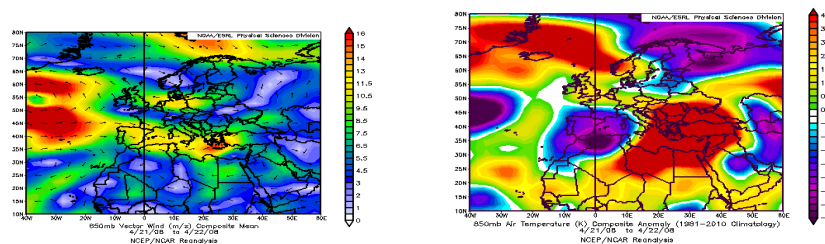
7

8

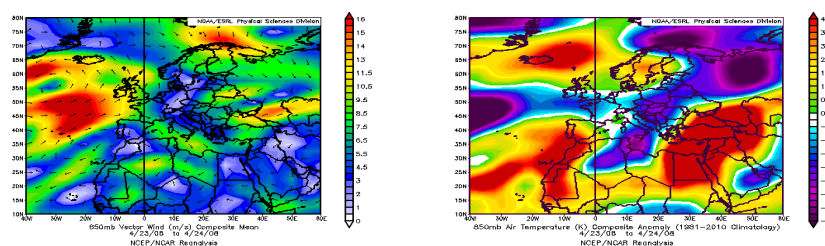
9



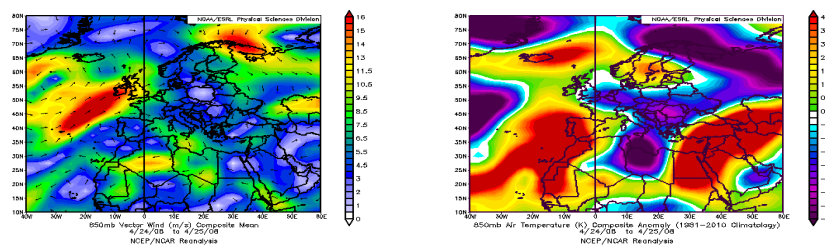
1



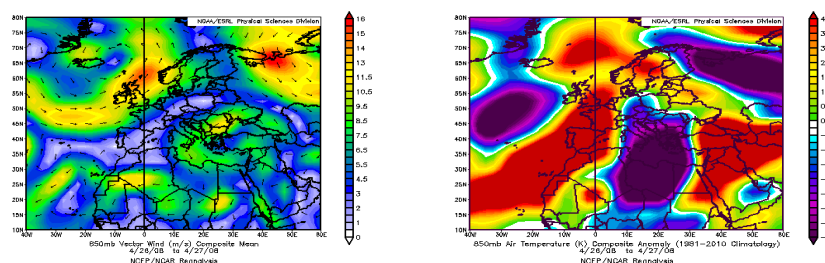
2



3



4



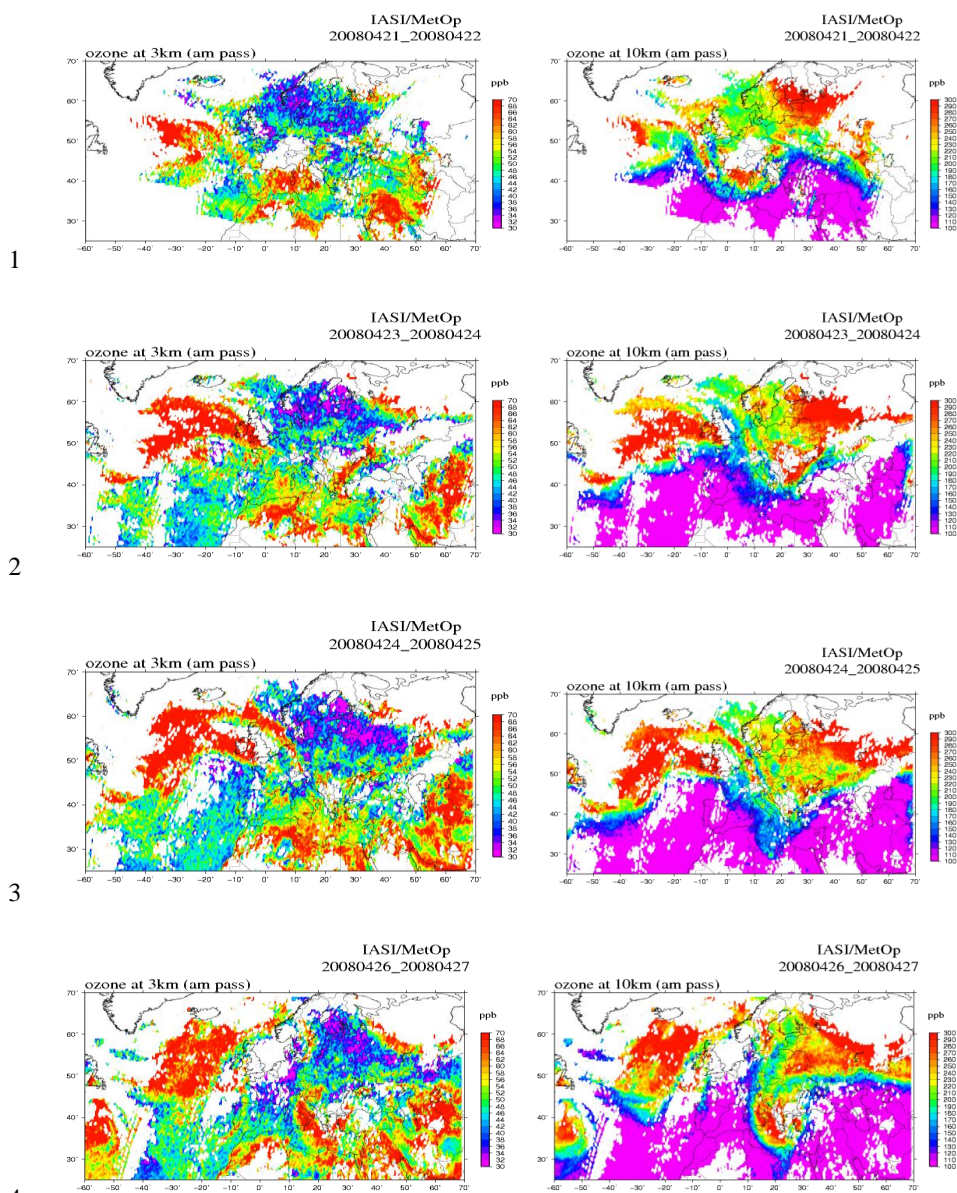
5 **Figure 4: Same as Fig. 2 but for vector wind (left column) and air temperature anomaly (right column).**

6

7

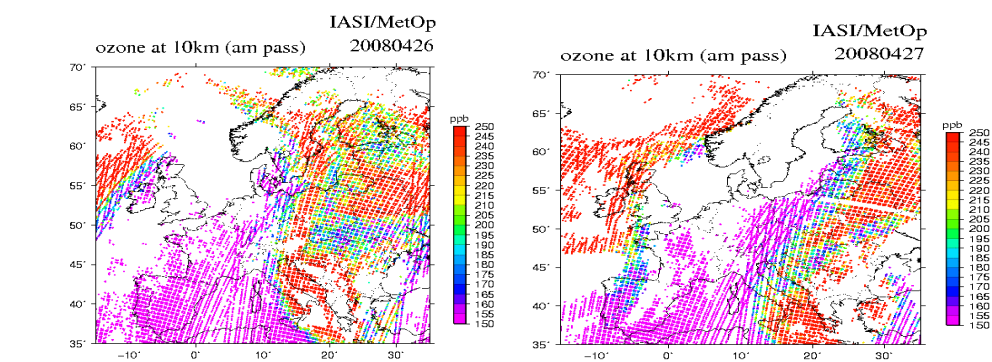
8

9

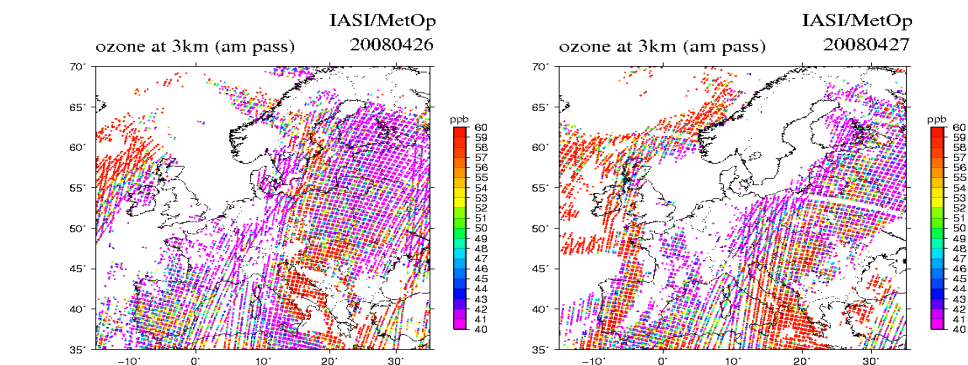


5 **Figure 5: IASI satellite ozone measurements at 3km level (left column) and 10 km level (right column)**
6 **during the high ozone episode of 26-27 April 2008 (lowest panels) as well as for two, three and five days**
7 **before. Values outside the scale range are set up to the upper and lower color code respectively.**

8
9



1



2

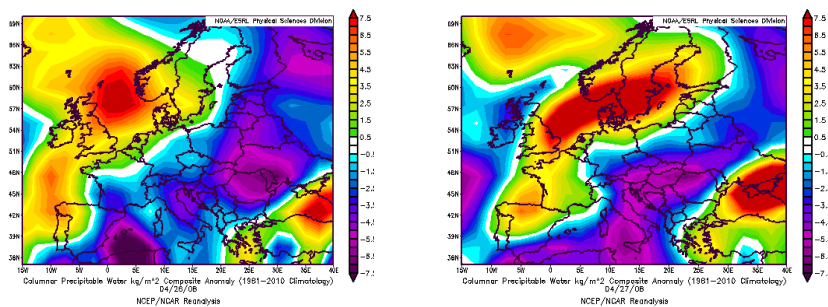
3 **Figure 6: Daily IASI satellite ozone measurements at 10 km level (upper panel) and at 3km level (lower**
4 **panel) for April 26, 2008 (left column) and April 27, 2008 (right column). Values outside the scale range**
5 **are set up to the upper and lower color code respectively.**

6

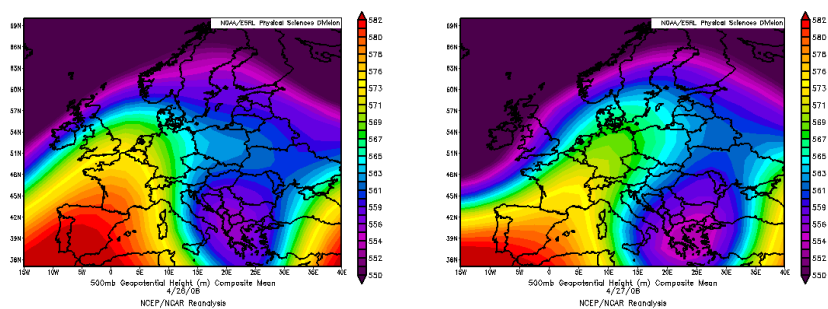
7



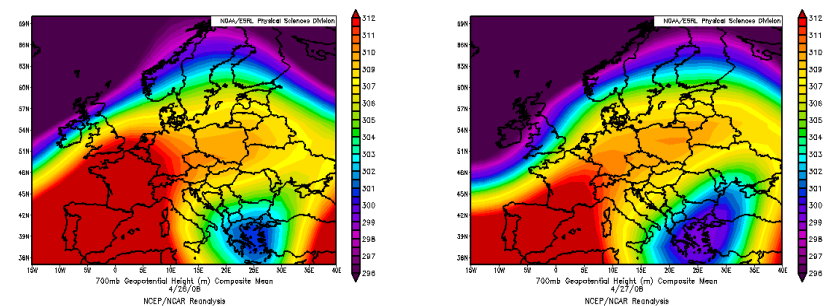
1



2



3



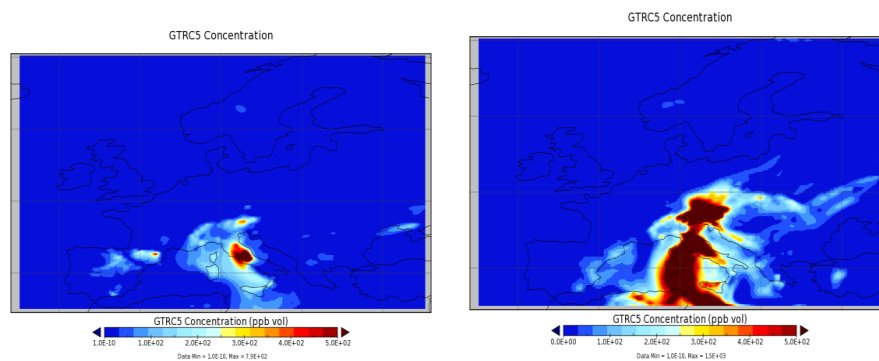
4

5 **Figure 7: Columnar precipitable water anomaly (upper panel), geopotential height at 500hPa (middle**
6 **panel) and geopotential height at 700hPa (lower panel) for April 26, 2008 (left column) and April 27, 2008**
7 **(right column).**

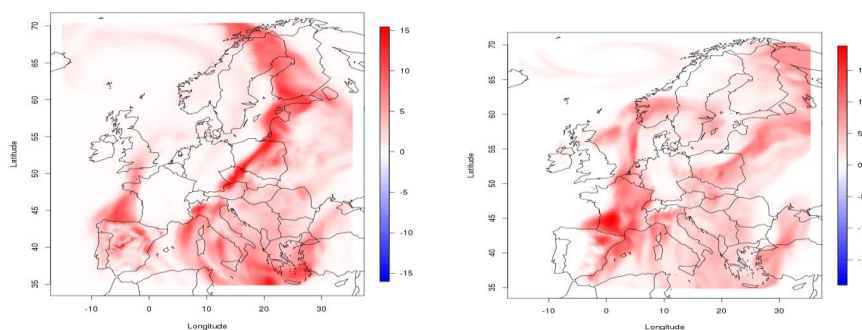
8



1



2



3

4 **Figure 8 (Upper panel): CHIMERE simulations of upper tropospheric tracer concentrations at 3 km for**
5 **April 26, 2008 (left column) and for April 27, 2008 (right column).**

6 **(Lower panel): CHIMERE simulations of photochemical production (difference between the reference**
7 **simulation and a simulation without emissions) at 3km (in ppb) for April 26, 2008 (left column) and for**
8 **April 27, 2008 (Right column).**

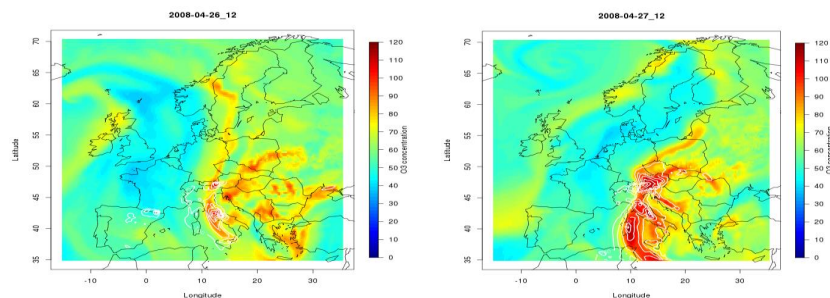
9

10

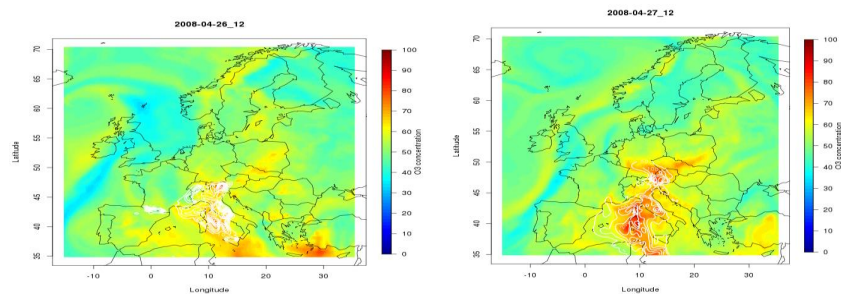
11



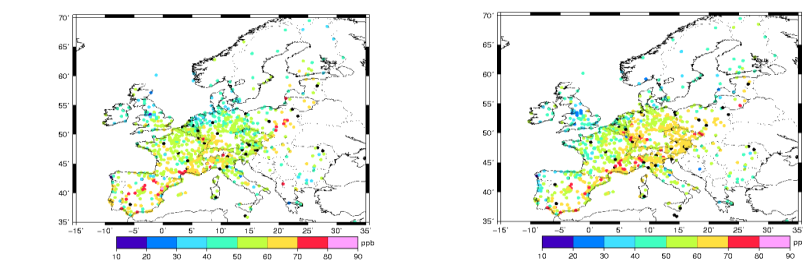
1



2



3



4

5 **Figure 9 (Upper panel):** CHIMERE simulations of the ozone field at 3 km altitude (in ppb) with the iso-
6 contours of the high tropospheric tracer (in white, arbitrary units) for April 26, 2008 (left column) and for
7 April 27, 2008 (right column). (Middle panel): Same as in upper panel but for 1.5 km altitude. (Lower
8 panel): Hourly average surface ozone (EEA-AirBase) mixing ratios (ppb) at 15:00 h for April 26, 2008
9 and for April 27, 2008 (right column). Ozone data are from the EEA-AirBase database.

10



1

2

3

4

5

6

7

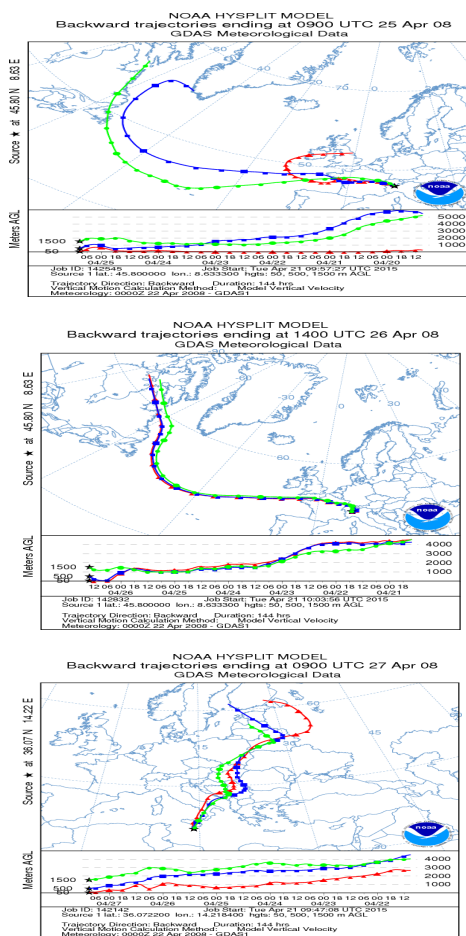


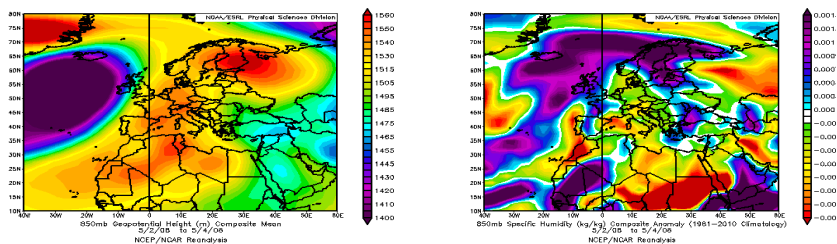
Figure 10: Backward trajectories during the April 25-27 episode ending at EMEP rural ozone stations in Italy (IT04, upper and middle panels) and Malta (MT01, lower panel).



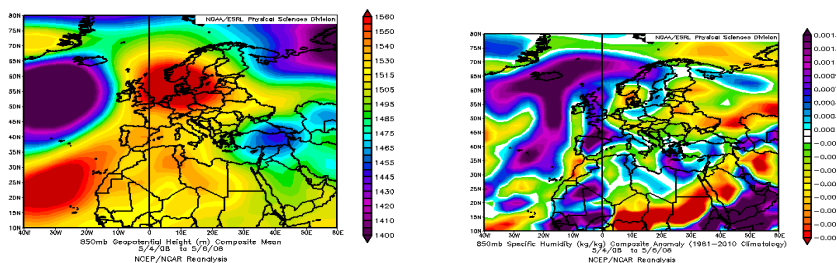
1

2

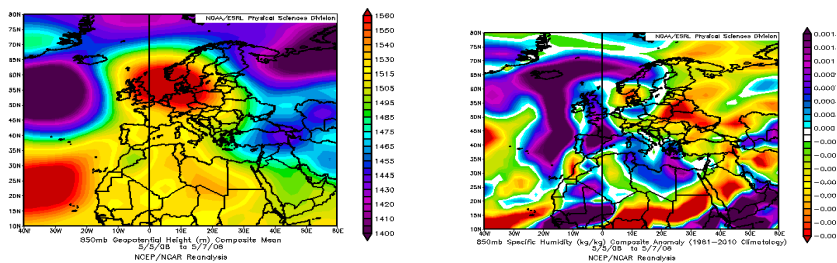
3



4



5

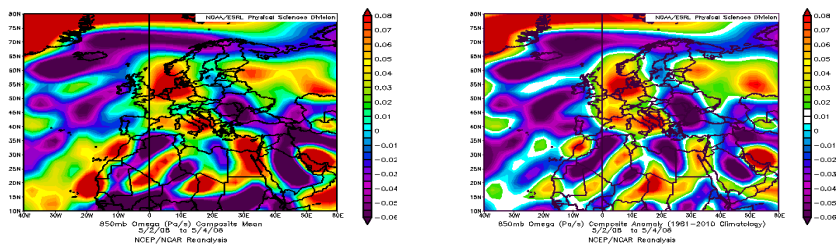


6

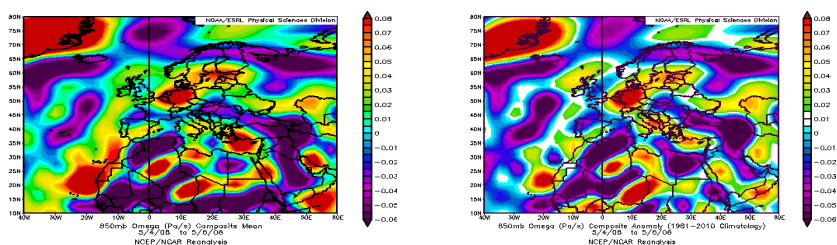
7 **Figure 11: Composite weather maps of geopotential height (left column)**
8 **and specific humidity (right column), for the high ozone episode of 7-9 May 2008 (lowest panels) as well as for two, three and five days**
9 **before.**



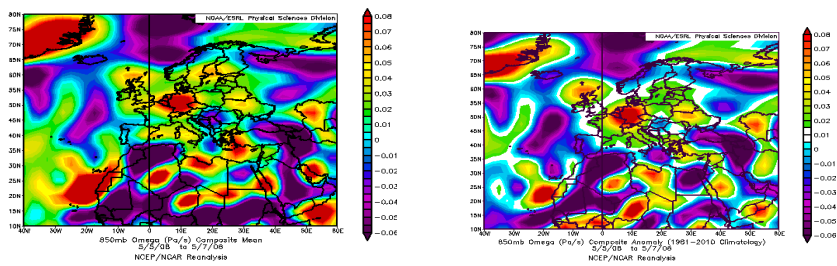
1



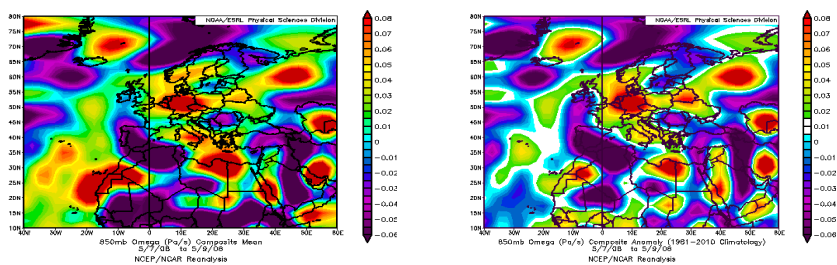
2



3



4



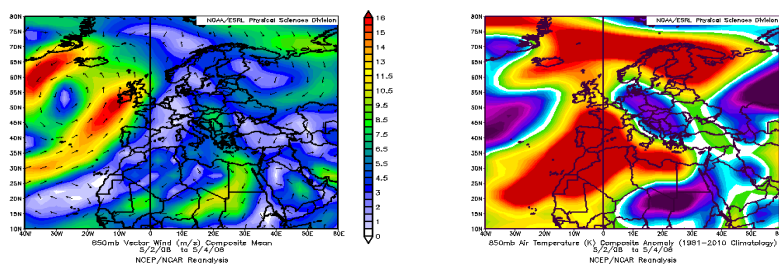
5

6 **Figure 12: Same as Fig. 8 but for omega vertical velocity (left column) and omega vertical velocity**
7 **anomaly (right column).**

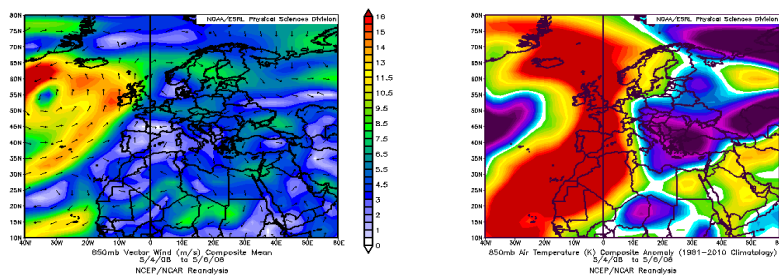
8



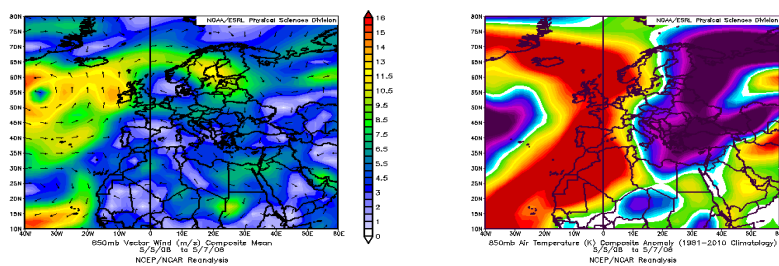
1



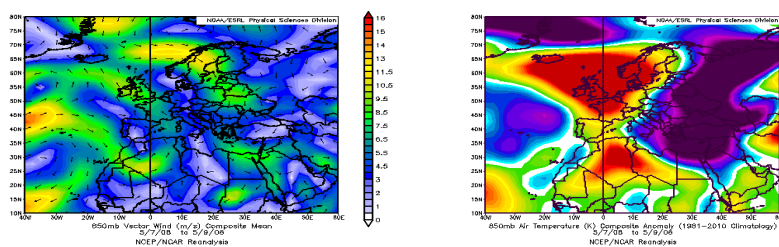
2



3



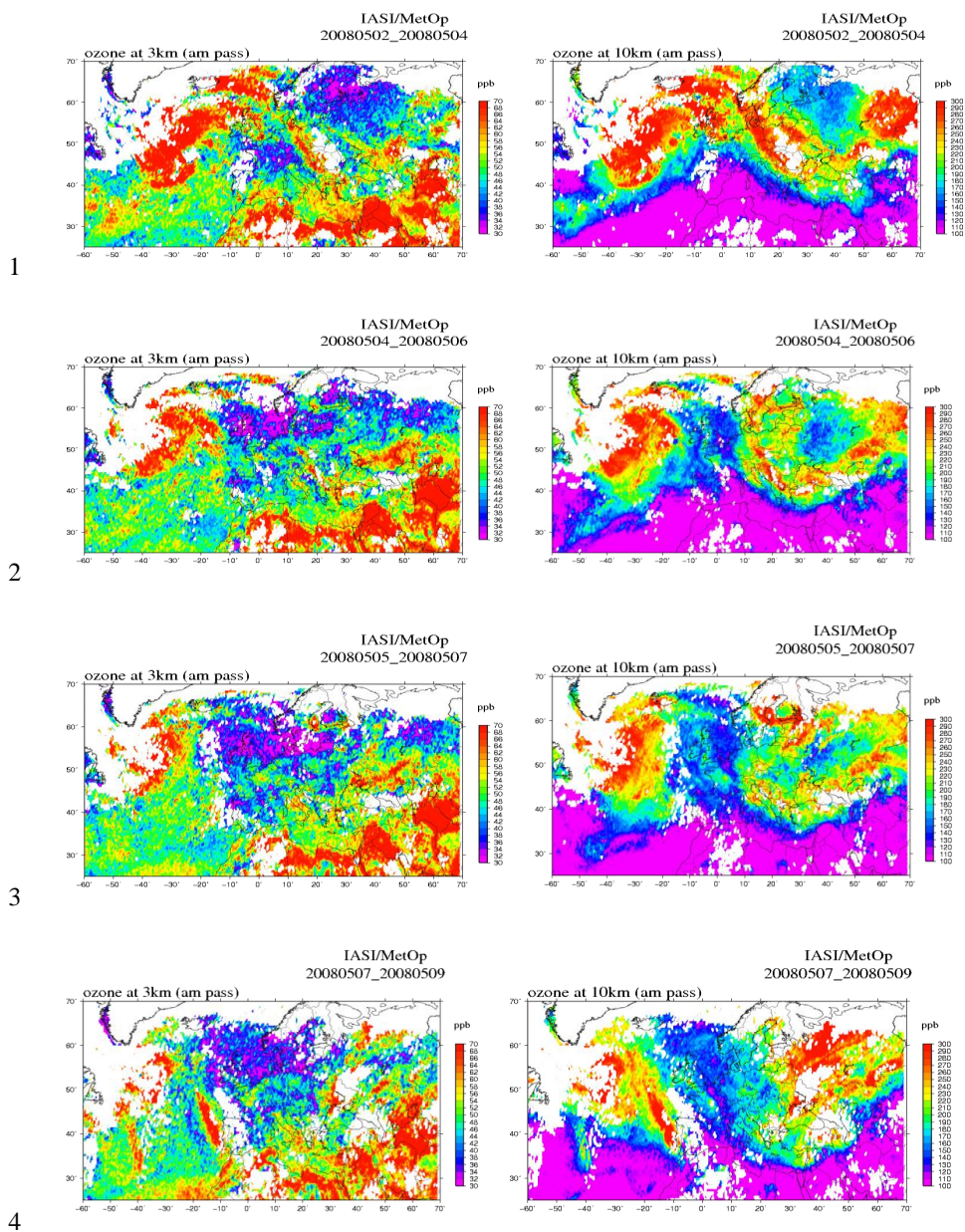
4



5

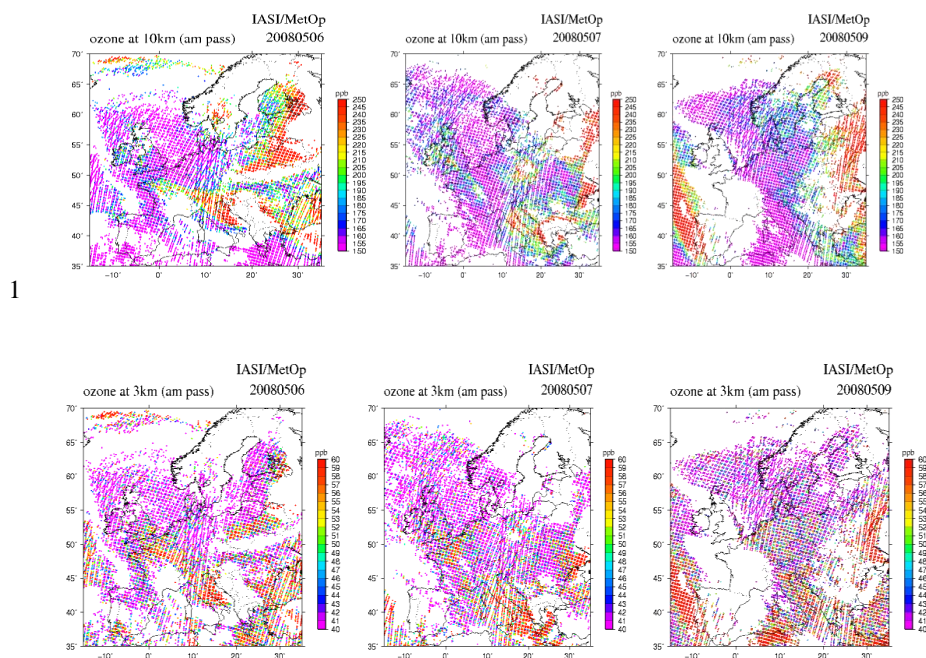
6 **Figure 13: Same as Fig. 8 but for vector wind (left column) and air temperature (right column).**

7



1
2
3
4
5 **Figure 14: IASI satellite ozone measurements at 3km level (left column) and 10 km level (right column)**
6 **during the high ozone episode of 7-9 May 2008 (lowest panels) as well as for two, three and five days**
7 **before. Values outside the scale range are set up to the upper and lower color code respectively.**

8



1

2

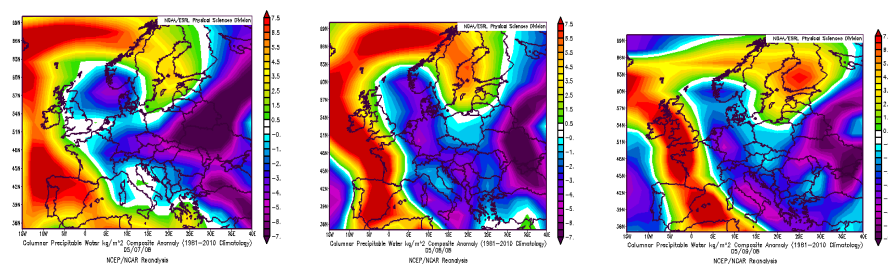
3 **Figure 15: Daily IASI satellite ozone measurements at 10 km level (upper panel) and at 3km level (lower**
4 **panel) for May 6, 2008 (left column), May 7, 2008 (middle column) and May 9, 2008 (right column).**
5 **Values outside the scale range are set up to the upper and lower color code respectively.**

6

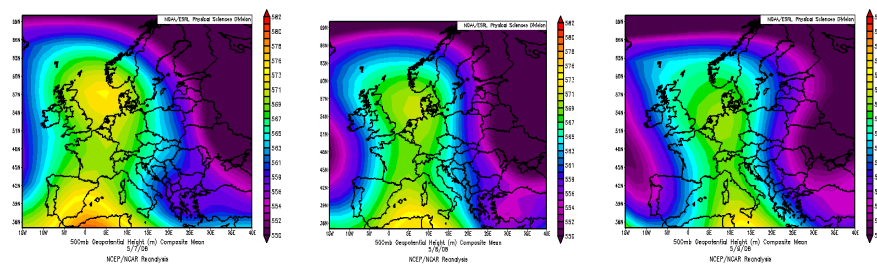


1

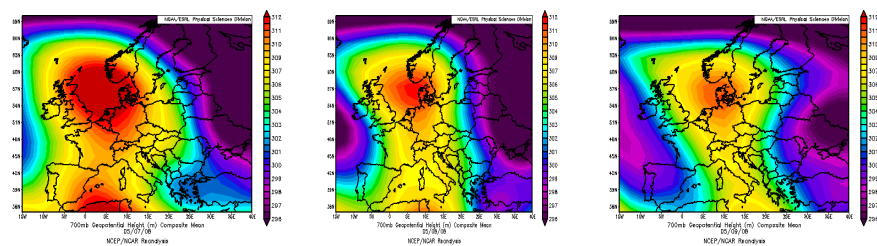
2



3



4



5

6 **Figure 16: Precipitable water anomaly (upper panel), geopotential height at 500hPa (middle panel) and**
7 **geopotential height at 700hPa (lower panel) for May 7, 2008 (left column), May 8, 2008 (middle column)**
8 **and May 9, 2008 (right column).**

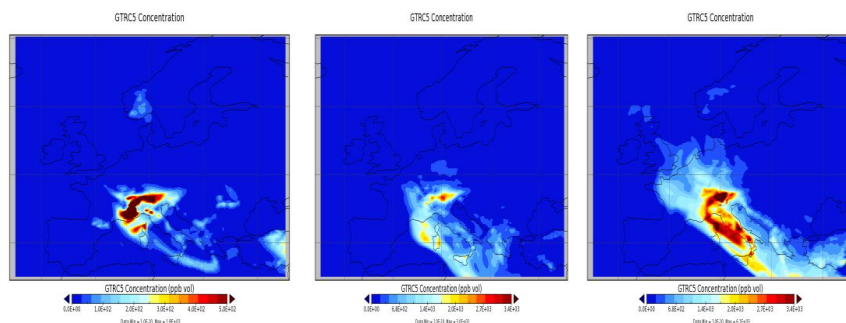
9

10

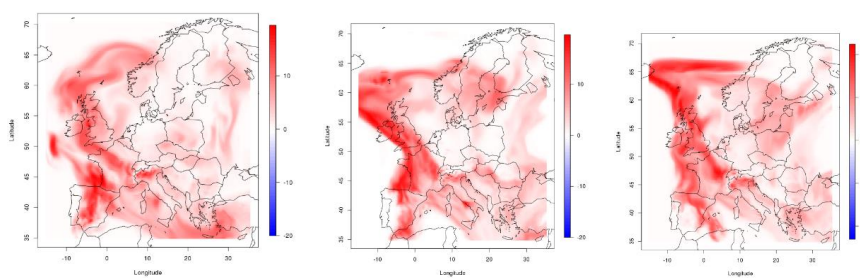
11



1



2



3

4

5 **Figure 17 (Upper panel): CHIMERE simulations of upper tropospheric tracer concentrations at 3 km**
6 **for May 7, 2008 (left), May 8, 2008 (middle) and for May 9, 2008 (right).**

7 **(Lower panel): CHIMERE simulations of photochemical production (difference between the reference**
8 **simulation and a simulation without emissions) at 3km (in ppb) for May 7, 2008 (left), May 8, 2008**
9 **(middle) and for May 9, 2008 (right).**

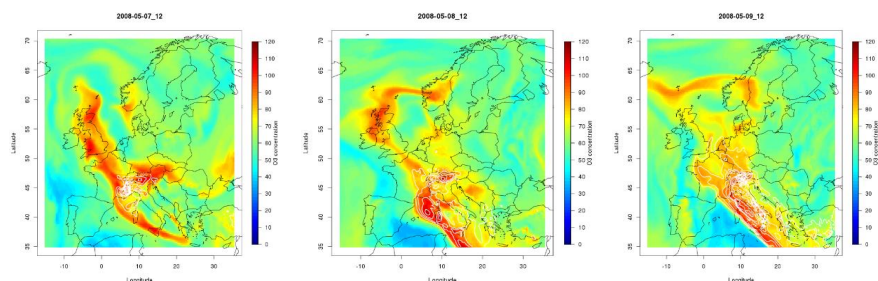
10

11

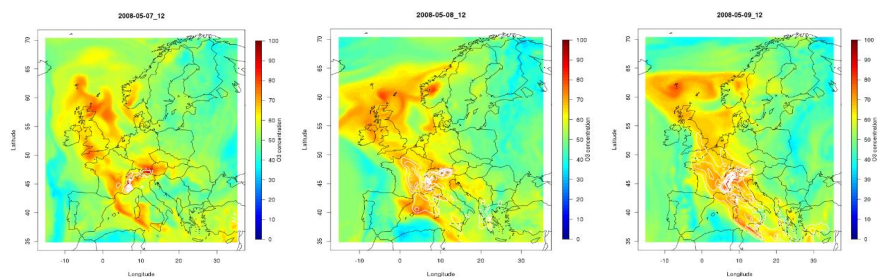
12



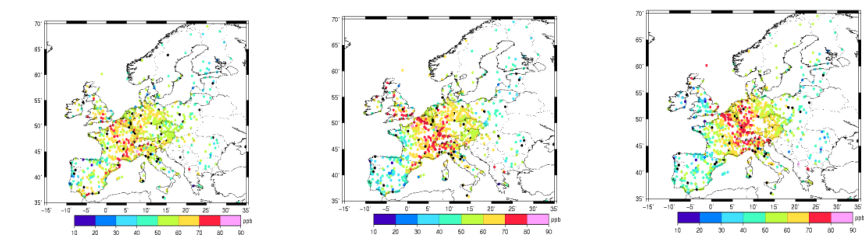
1



2



3



4

5 **Figure 18 (Upper panel):** CHIMERE simulations of the ozone field at 3 km altitude (in ppb) with the iso-
6 contours of the high tropospheric tracer (in white, arbitrary units) for May 7, 2008 (left column), May 8,
7 2008 (middle column) and May 9, 2008 (right column). (Middle panel): Same as in upper panel but for 1.5
8 km altitude. (Lower panel): Hourly average surface ozone (EEA-AirBase) mixing ratios (ppb) at 15:00 h
9 for May 7, 2008 (left column), May 8, 2008 (middle column) and May 9, 2008 (right column). Ozone data
10 are from the EEA-AirBase database.

11

12

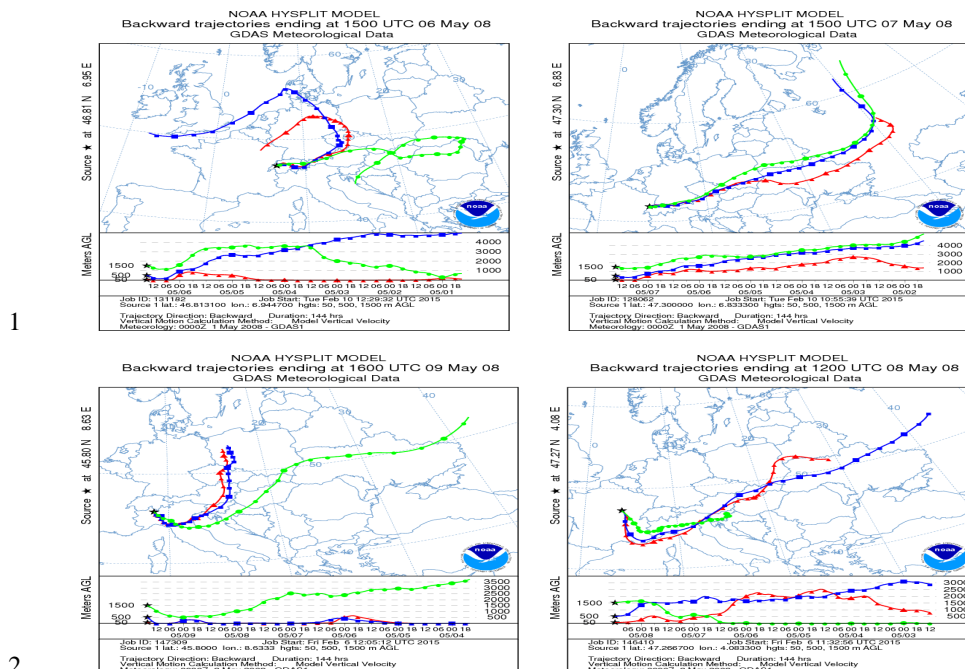
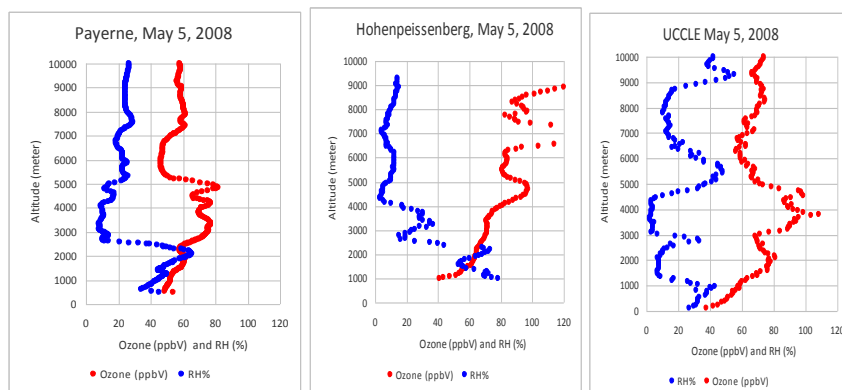


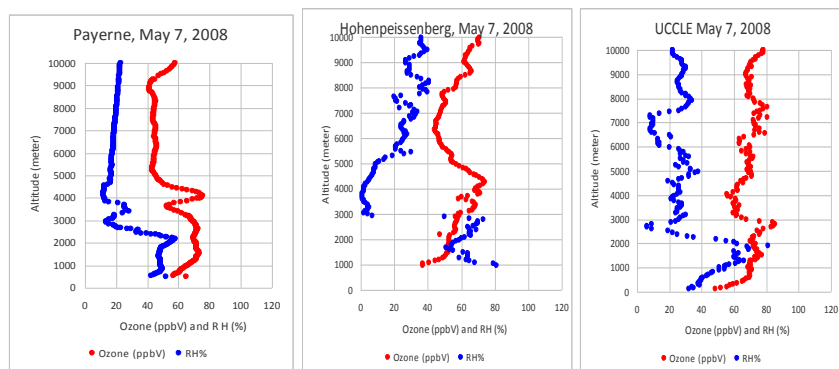
Figure 19: Backward trajectories during the 6-9 May 2008 ozone episode ending at EMEP rural ozone stations in Switzerland and Italy (left column) and France (right column).



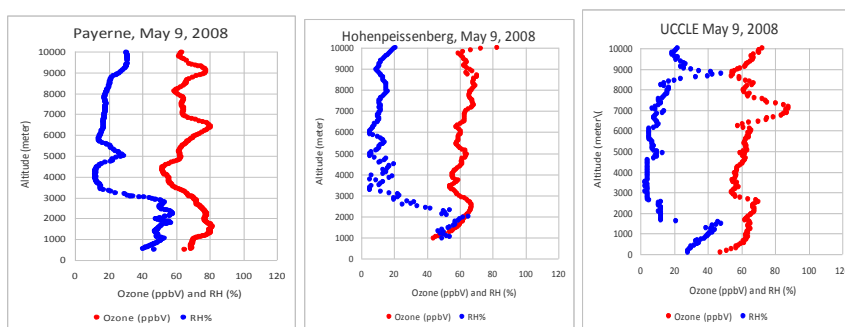
1



2



3



4

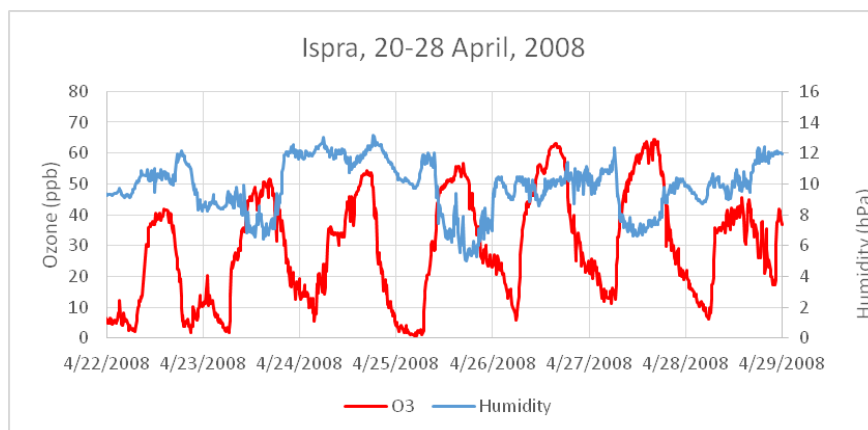
5 **Figure 20: Vertical profiles of ozone (red) and relative humidity (blue) over Payerne, Switzerland (left**
6 **column), Hohenpeissenberg, Germany (middle column) and Uccle, Belgium (right column) on May 7,**
7 **2008 (upper panel), May 8, 2008 (middle panel) and May 9, 2008 (lower panel).**

8

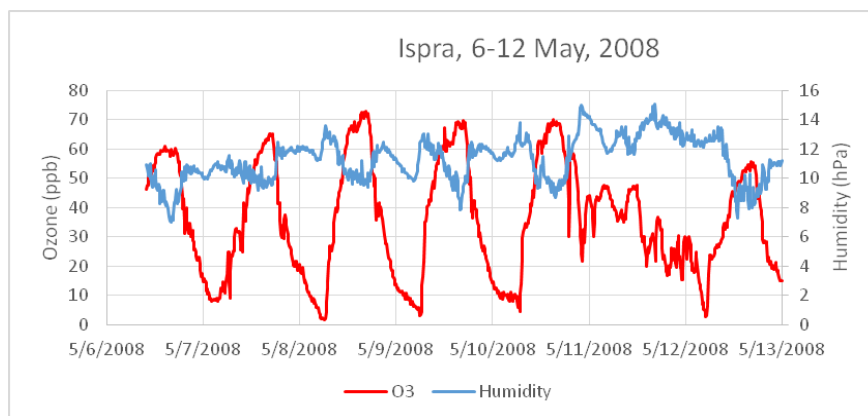
9



1



2



3

4

5 **Figure 21: (Upper panel): Ozone concentration (red) and absolute humidity (blue) measurements at the**
6 **JRC-Ispra station during the 26-27 April 2008 ozone episode.**

7 **(Lower panel): Ozone concentration (red) and absolute humidity (blue) measurements at the JRC-Ispra**
8 **station during the May 7-9, 2008 ozone episode.**